8-2003

Determination of Mechanical Properties of Treated Wood using Near Infrared Spectroscopy

Stephen E. Hedrick II
University of Tennessee - Knoxville

To the Graduate Council:

I am submitting herewith a thesis written by Stephen E. Hedrick II entitled "Determination of Mechanical Properties of Treated Wood using Near Infrared Spectroscopy." I have examined the final electronic copy of this thesis for form and content and recommend that it be accepted in partial fulfillment of the requirements for the degree of Master of Science, with a major in Civil Engineering.

Richard M. Bennett, Major Professor

We have read this thesis and recommend its acceptance:

Timothy G. Rials, Edwin G. Burdette

Accepted for the Council:
Carolyn R. Hodges

Vice Provost and Dean of the Graduate School

(Original signatures are on file with official student records.)

To the Graduate Council:

I am submitting herewith a thesis written by Stephen E. Hedrick II entitled "Determination of Mechanical Properties of Treated Wood using Near Infrared Spectroscopy." I have examined the final electronic copy of this thesis for form and content and recommend that it be accepted in partial fulfillment of the requirements for the degree of Master of Science, with a major in Civil Engineering.

Richard M. Bennett

Dr. Richard M. Bennett
Major Professor

We have read this thesis
and recommend it acceptance:

Timothy G. Rials

Dr. Timothy G. Rials

Edwin G. Burdette

Dr. Edwin G. Burdette

Accepted for the Council:

Dr. Anne Mayhew

Vice Provost and
Dean of Graduate Studies

(Original signatures are on file with official student records.)

DETERMINATION OF MECHANICAL PROPERTIES OF TREATED WOOD USING NEAR INFRARED SPECTROSCOPY

A Thesis
Presented for the
Master of Science
Degree
The University of Tennessee, Knoxville

Stephen Edward Hedrick II
August 2003

ACKNOWLEDGEMENTS

I would like to extend my thanks to all of those who helped me in completing my Master of Science in Civil Engineering. I would like to thank my major professor, Dr. Richard M. Bennett for all of his guidance and effort in helping me complete this undertaking. I would like to thank Dr. Timothy G. Rials for his guidance in making me familiar with the concepts of Near Infrared Spectroscopy. I would like to thank Dr. Stephen S. Kelley for his help with the statistical analysis and any other questions that I had. I would also like to thank Dr. Edwin G. Burdette for service in my committee.

ABSTRACT

The purpose of this study was to determine the mechanical properties of treated wood using near infrared spectroscopy. This nondestructive evaluation was used to analyze the tensile strength parallel to the grain, modulus of elasticity parallel to the grain and creosote content of a southern pine telephone pole removed from service. Tests were conducted on tensile samples that were cut from sections of the pole in order to determine the actual values. Partial least squared models developed with reduced wavelengths and models developed from several 50 nanometer (nm) intervals along the spectrum showed promise in the prediction of these properties. The results show the potential value of Near Infrared (NIR) spectroscopy as a feasible, nondestructive way of determining the mechanical properties of treated wood.

TABLE OF CONTENTS

Chapter **Page**

LIST OF TABLES

Table **Page**

LIST OF FIGURES

CHAPTER 1
INTRODUCTION

1.1 Background

The design requirements of timber construction used in the transportation and utility industries, such as bridges and utility poles, require an effective maintenance program to ensure safe and reliable service. As such, preservative-treated timber, rather than naturally durable timber, is required in order to obtain adequate performance.

Typically pole replacement is neither easy nor economical. Poles treated with preservatives, creosote and pentachlorophenal, are considered hazardous waste in some states. Some landfills will not accept hazardous material thus other more costly disposal methods must be employed. Over the years, the need for effective non-destructive evaluation (NDE) for the strength of timber has grown as the costs for quality timber has risen. There are approximately 150 million wood utility poles in service carrying electrical transmission and distribution lines. Each year, the ever-expanding basic electric and communication industries consume about 6 million treated poles. Approximately 75 percent of the annual consumption of the poles consist of southern yellow pine (*Pinus* spp.) (Micklewright 1989). Creosote was used in 17 percent of the United States pole production (11 million ft.3) in 1993 and part of this volume was exported. About 1 to 2 million poles are being replaced each year (AWPI 1994).

Extending service life, while maintaining reliability is being increasingly emphasized. Methods have been developed based on the sonic resonance properties of the wood in order to predict wood properties (Ross 1999). These methods detect defects by sonic wave velocity, acoustic emission and stress wave analysis. The disadvantage to

these methods is that, once a defect is detected, other methods must still be used to determine the cause. X-rays and tomography scanners have also been used to detect defects; however, these techniques have been phased out due to high cost and safety concerns with radiation (Ritter 1990). One technique that has promise is the use of Near Infrared (NIR) spectroscopy. NIR spectroscopy uses a fiber optic probe to quantify the amount of near infrared light absorbed by a material.

Near Infrared spectroscopy has been in application over the past several years, in such industries as chemicals, pharmaceuticals and food. It has been an effective means in determining the chemical composition of various materials. Recent applications of NIR have been in determining the chemical structure of such materials as paper, wood and various other biobased materials. The chemical makeup of such materials can be determined by other various spectroscopic techniques. However, NIR spectroscopy has advantages that are available including minimal sample preparation, fast acquisition times, non-destructive sampling, and the potential for on-line or portable applications. In the past, advancement in the use of NIR has been hindered due to the broad and poorly defined peaks, which exemplify this particular region of the spectrum. Recent developments in multivariate analysis (MVA) statistical techniques have created a more reachable means of obtaining the chemical information that is contained within the NIR spectrum. The use of MVA has developed the use of NIR data towards physical and mechanical property modeling, which is significantly past the strict chemical composition considerations of the past. In several recent publications the prospective value of using NIR for monitoring wood properties has been demonstrated (as qtd. in Rials).

The use of this technique, however, is not limited to in-service utility poles. NIR spectroscopy could be used for determining properties of out-of-service utility poles, in order to establish suitability for other external uses such as fence posts, retaining walls, landscaping timbers and other general structural applications.

1.2 Objective

The purpose of this study was to determine the feasibility of using Near Infrared spectroscopy to predict the mechanical properties of creosote treated wood. To accomplish this, partial least squares regression models were created to simulate lightweight, less expensive spectrometers. The results from these models were compared to the results from the full spectral model in order to determine the losses or gains in accuracy with the use of such spectrometers.

CHAPTER 2
PROCEDURES

2.1 Materials

Two portions of out-of-service utility poles were obtained from a local company that markets these poles to be used as fence posts, pole barns and other non-essential structures. These poles were determined to be creosote-treated, southern yellow pine (*Pinus taeda*). Neither the age of the poles nor how long they had been out of service was known. Each pole was approximately eight feet in length and ten inches in diameter. It was assumed that the portions obtained were from the lower portion of the utility poles, based on the amount of nails and staples present in the poles.

2.2 Sample Preparation

The tensile test specimen of ASTM D1037 was chosen as opposed to the ASTM D143 due to the time requirements in the preparation of each specimen along with the availability of an extensometer that would readily fit the specimen of the ASTM D1037. The dimensions of the specimens were based on the Tensile Strength Parallel to Surface in ASTM D1037. The length of each specimen was modified in order to accommodate the extensometer's gage length of four inches. Preliminary tests resulted in many of the specimens fracturing outside of the gage length or in the grip area of the specimen; therefore, the data were not valid. In order to correct this problem, the thickness of the middle section was narrowed to one eighth of an inch. The width of the middle section of the specimens was narrowed to three quarters of an inch. After these modifications were

made, the specimens regularly fractured inside the gage length. The final dimensions of the specimens as tested are shown Figure 2.1.

There are two different types of cell structures present in wood. Early-wood cells are those that form in the first or second months of the growing season. These cells have relatively large cavities and thin walls. The cells that form later in the growing season are latewood cells. These have smaller cell cavities and thicker walls in comparison to the early-wood cells (Ritter 1990). These two cell structures form the growth rings within a tree. Early-wood creates the lighter color, while latewood creates the darker color. Due to the differences in the two cell structures, early-wood and late-wood have significantly different mechanical properties. In order to prevent the specimens from being dominated by the properties of either the early-wood or late-wood, the specimens were cut in the radial direction. By cutting the specimens radially, there was approximately an even amount of both earlywood and latewood present.

Numerous tensile test specimens were made from the utility poles. Therefore, a numbering system was developed that would identify the precise location on the utility pole from which the specimen originated. The specimens were labeled according to the following format:

A – B – C – DD

where,

A = Pole Number,
B = Segment on the Pole,
C = 1 – inner portion of segment,
2 – outer portion of segment,
DD = Location on segment (Figure 2.2).

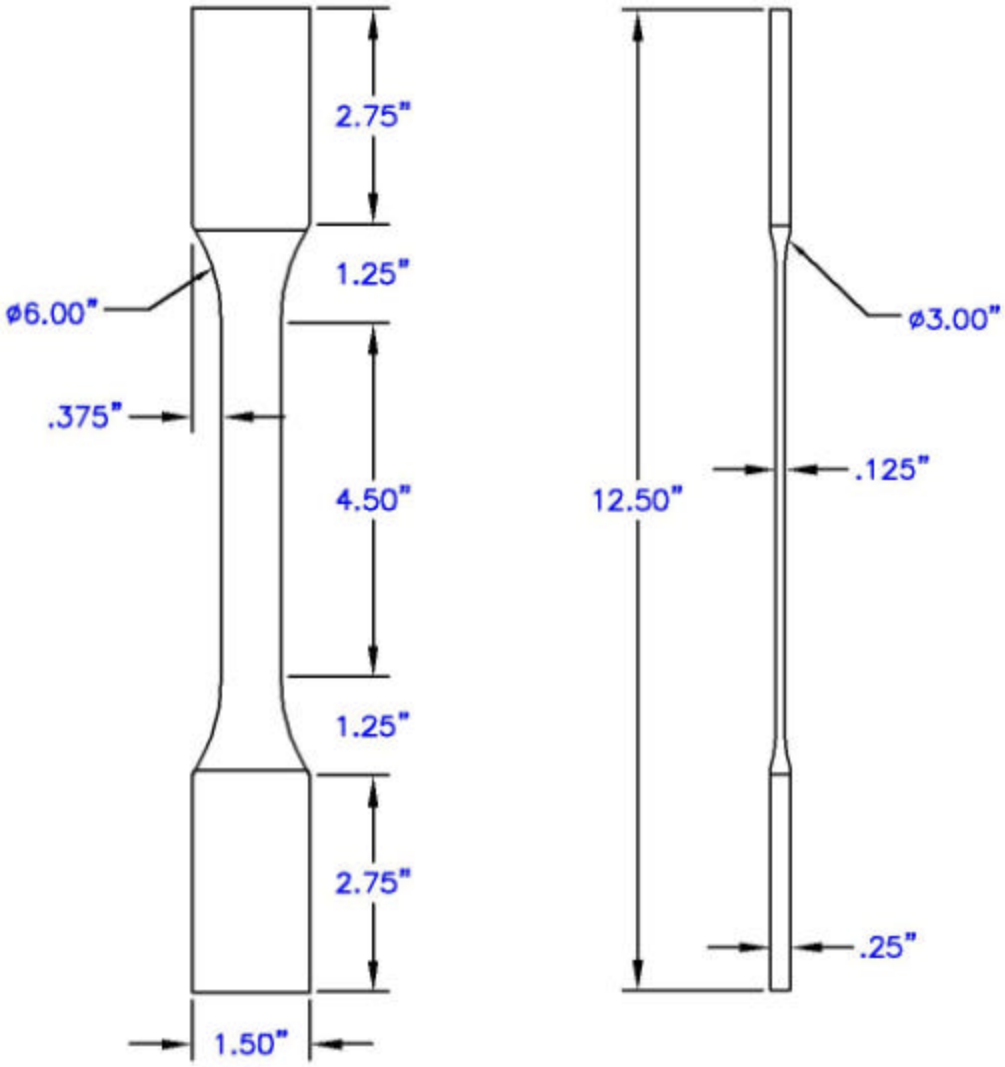

Figure 2.1 – Modified dimensions of tensile test specimen.

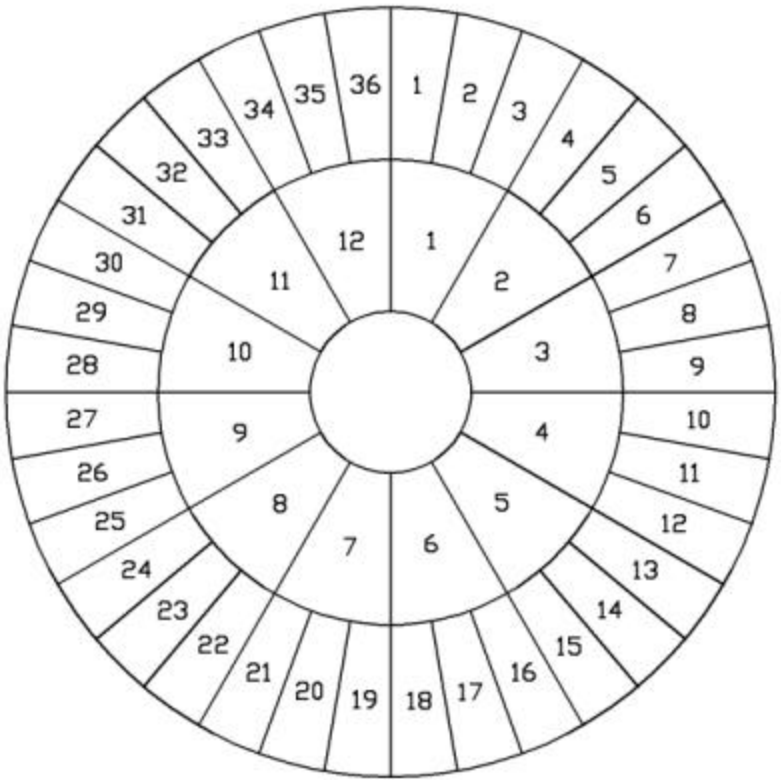

Figure 2.2 – Illustration of labeling system developed for location of specimen on the cross section.

The following steps outline the procedure involved in the preparation of the specimens:

1. The pole was cleaned with a pressure washer. All nails, staples and any other foreign objects were removed.
2. Telephone pole was cut transversely every fourteen inches (14") along the longitudinal axis with a horizontal band saw. Each section was numbered sequentially.
3. Each section was cut in half along the longitudinal axis with the use of a resaw band saw.
4. Each half was cut in half along the longitudinal axis on the resaw band saw. The segment was "quartered" at this point.
5. Both ends of the "quarter" were marked into three thirty-degree (30^{o}) wedges. The three wedges were cut out on the resaw band saw.
6. One side of each wedge was run through a jointer until a flat surface was obtained.
7. The wedge was ripped on a table saw. The flat surface was placed on the table saw and the outside of the wedge was placed along the fence. The wedge was ripped in order to leave a minimal inner height of three-eighths of an inch (3/8").
8. The blade of the table saw was adjusted to fifteen degrees (15^{o}) and the fence was set to cut a width of one and five-eighths inches (1-5/8"). The wedges were ripped with the inner edge guided along the fence.
9. At this point, the wedge was in two segments, an inner and outer portion. One side of the outer portion was run through the jointer until the surface became perpendicular to the inner edge.
10. The inner and outer portions were ripped to three-eighths of an inch (3/8") strips along the longitudinal axis with the resaw band saw. Three specimens should be obtained from the outer portion and one specimen obtained from the inner portion. All specimens were marked with their appropriate number.
11. One longitudinal face of the specimens was planed until a smooth surface was obtained using a thickness planar.
12. The opposite longitudinal face of the specimen was planed to a final thickness of one-quarter of an inch (1/4") with the thickness planar.
13. One longitudinal edge of the specimens was squared on the jointer.
14. The specimens were ripped to their final width of one and a half inches (1-1/2") on the table saw, with the squared edge along the fence.
15. The specimens were cross cut on a radial arm saw to their final length of twelve and one half inches (12-1/2").
16. The width of the middle portion of the specimens was reduced by first forming coves at each end of the reduced width portion and then removing the wood in the middle. To form the cove, the guard was removed from the table saw. The height of the table saw blade was set to three eighths of an inch (3/8"). A straight edge was clamped to the top surface of the table saw. The straight edge was set at approximately forty two degrees to the saw blade and also so that the perpendicular distance from the straight edge to the point that the saw blade breaks the surface of the table was two and three quarters of an inch (2-3/4"). Test samples were run until the length of the cove was two and a half inches (2-

1/2”). The length of the cove was altered by adjusting the angle the straight edge and the saw blade. The specimens were run across the saw blade perpendicular to the straight edge with the end of the specimen against the straight edge. This was done four times on each specimen. A fine-toothed saw blade was used for this cut to insure a smooth finish.

17. A dado blade was set up in the table saw and adjusted to a height of three-eighths of an inch (3/8”). The four and one half inches (4-1/2”) of material between the cove cuts was removed to create a specimen width of three quarters of an inch (3/4”).
18. To reduce the thickness of the specimen, a oscillating drum sander was set up with a three-inch diameter drum with sixty-grit sand paper. A fence was clamped to the base of the drum sander as to allow a sixteenth inch (1/16”) of material along the middle four and one half inches to be removed on each side of the specimen; resulting in a specimen thickness of one eighth of an inch (1/8”).

After the specimens had been cut, they were set aside for a period of one week, in order to allow consistent moisture content to be reached. This consistency was obtained once the moisture content of the specimens reached equilibrium with the moisture content of the surrounding environment. The average moisture content of all specimens was eleven and one-half percent (11.5%).

2.3 Near Infrared Spectroscopy

Near Infrared (NIR) reflectance spectra were obtained from four locations along the radial-longitudinal face of each specimen using a LabSpec Pro® Near Infrared Spectrometer. The Near Infrared Spectrometer was equipped with a naked fiber optic probe. The fiber optic probe scans an area with a diameter that is half the distance between the probe and the surface of the specimen. To scan the three quarters of an inch wide specimen, the fiber optic probe was placed perpendicular to the surface of the specimen at a distance of one and a half inches above the sample. An incandescent lamp was positioned so that it would illuminate the area of the specimen to be scanned at an

angle of thirty degrees from horizontal. Of the four scans taken, two scans were taken from each side of the specimen, with each scan being approximately one and a half inches from the center of the specimen as illustrated in Figure 2.3. These scans were taken at these approximate locations, due to the fact the specimen would break somewhere along the middle of the structure. The spectra were collected at 1-nm intervals over the wavelength range 350-2500 nm. Due to multiple scans being taken, it proved more time efficient to set up an automatic timer that would scan the specimen within a specific time interval. A period of eight seconds was found to be a productive work pace.

2.4 Tensile Testing

Once the specimens were scanned, the tensile strength parallel to the grain was obtained. An extensometer was clamped onto the specimen to measure the elongation of the specimen as it undergoes testing. The extensometer consisted of two Linear Variable Differential Transformers (LVDT) that measured elongations, along with two clamping points that determined the gage length. The gage length represented the distance over which the deformation was measured, and was four inches for the extensometer used (Figure 2.4). Two LVDT's were used to cancel out any accidental bending that might occur in the specimen.

The specimen was placed into wedge grips that were attached to the crossheads of the loading machine. Wedge grips were used in order to assure that the specimen did not slip while undergoing testing. The grips should not be placed any closer than one quarter of an inch to the tapered area of the specimen. If the grips were placed too close to the

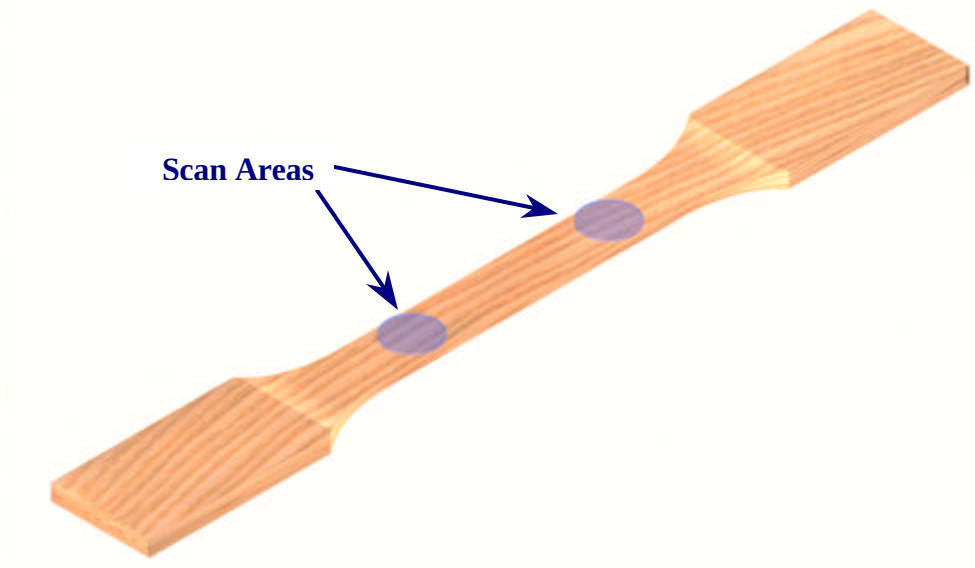

Figure 2.3 – Illustrations demonstrating locations from where Near Infrared spectra was collected.

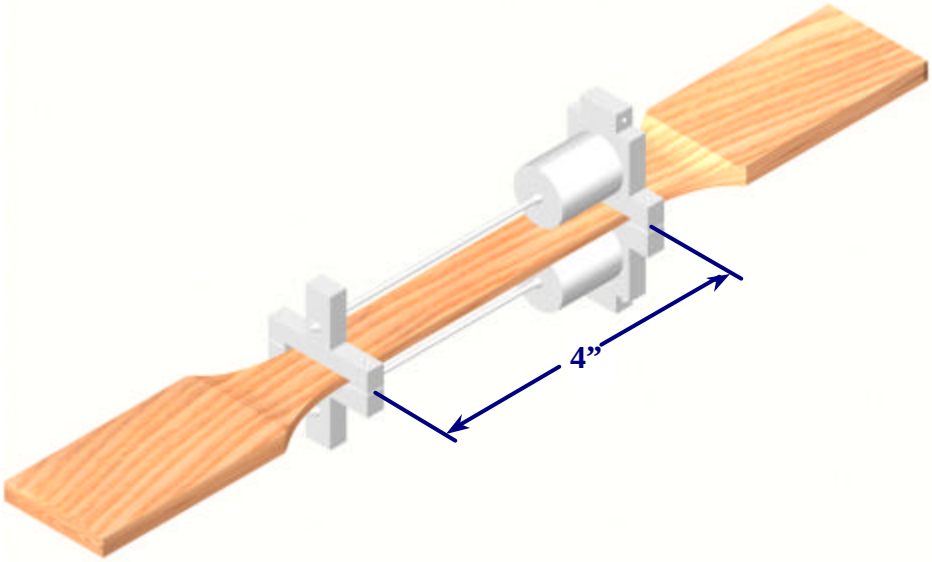

Figure 2.4 – Illustration of extensometer with four-inch gage length attached to tensile specimen.

tapered area, the specimens would tend to fracture in the area close to the grips. The loading apparatus and extensometer were operated by MTI® software. The specimen was continuously loaded at a uniform rate of 0.15 in./min as specified in ASTM D1037. Force and elongation data were automatically saved to a text file by the MTI® software.

2.5 Moisture Content

After tensile testing was complete, moisture content was determined as specified in ASTM D143. The specimens were initially weighed and placed into a 105° C oven for a period of 24 hours. Once removed from the oven the specimens' oven dried weight was recorded. The following equation was used to determine the specimens' moisture content:

$$\% \, MC = \frac{Int.Wt - OD\,Wt}{OD\,Wt} \times 100$$

where,

%MC = Moisture Content as a percentage.
Int. Wt. = Initial Weight of Specimen in grams.
OD Wt. = Oven Dried Weight of Specimen in grams.

2.6 Ground Samples

In using Near Infrared spectroscopy, the probe's capabilities were limited to detect only the properties on the surface of the specimen. Spectra were collected on ground specimens to determine if better correlations could be acquired. Additional work

was minimal since specimens needed to be ground to determine creosote content. A Wiley Mill equipped with a ½ millimeter mesh was used to grind each of the specimens. Approximately fifteen grams of grounds were obtained from each specimen. After the grinding was complete, two spectra were collected from each ground sample. Spectra were obtained the same as before, except, this time the ground samples were placed into a black metal bottle cap. The setup of a timer was once again beneficial in the productivity of the scanning process.

2.7 Creosote Content

By visual inspection, the creosote penetration varied from 1 to 3". Therefore, the level of creosote was higher in outer portions of the pole compared to the inner portions. This difference in creosote content was mainly due to bleeding and leaching. This phenomenon was caused by the surface of the pole being exposed to higher temperatures over the life of the pole than the interior, causing the evaporation mostly of low-molecular-weight fractions of the creosote. Thus, a pressure difference between the surface and interior of the pole occurs causing an outward movement of the creosote (Roliadi 2000). Since a difference in creosote content was present, it was advantageous to determine the effects of creosote content on the Near Infrared spectra. Creosote extractions were performed on the ground samples to evaluate the creosote content. This test was performed on 50 ground samples: 10 visually dark samples, 10 visually light samples, 10 low strength samples, 10 medium strength samples and 10 high strength samples.

Creosote extractions were performed approximately following ASTM D1860. Instead of extracting creosote and water, the samples were dried before the extraction took place. Therefore, any liquid extracted from the samples was assumed to be creosote. Creosote was extracted from the samples by the following steps:

1. Thimbles were weighed and weights recorded.
2. Approximately 5 grams of ground sample was placed into thimble.
3. Thimble and ground sample were dried in a vacuum-sealed oven at 65° C for a period of 12 hours. Initial oven-dried weight of thimble and ground sample was recorded.
4. About 200 mL of toluene was placed in a round bottom flask.
5. The thimble filled with the dried sample was placed inside an extraction flask. The extraction flask was placed on top of the round bottom flask and then a water-cooled condenser was placed on top of the extraction flask.
6. The whole apparatus was placed on a burner inside a vented hood.
7. Cold water was piped through the condenser and heat was applied to the apparatus so that the toluene boiled.
8. The system was allowed to reflux for at least 8 hours.
9. The thimble and sample was removed from the apparatus and allowed to air dry under a vented hood for 24 hours. After 24 hours, the thimble and sample were dried in a vacuum-sealed oven at 65°C for a period of 12 hours.

The percentage of creosote content was determined from the following equation:

$$\%C = \frac{C_1 - C_2}{C_2}$$

where,

%C = Percentage of Creosote Extracted,
C1 = Initial Oven Dry Weight of Sample in grams,
C2 = Final Oven Dry Weight of Sample in grams.

CHAPTER 3
RESULTS AND CONCLUSION

3.1 Statistical Analysis

Once all the spectrum and data were collected, statistical analysis was performed using The Unscrambler® version 7.6 (CAMO, Corvallis, OR) software in order to find correlations between the spectra and the physical properties of the wood. Three properties were considered: tensile strength parallel to the grain, modulus of elasticity parallel to the grain and percentage of creosote extraction.

Since the spectra were collected by reflectance mode, the spectrum was then converted from reflectance to absorbance. From each sample, four spectral readings were obtained. These four readings were averaged to obtain a single set of spectral data for each sample. The spectrum was collected at every nanometer. It was averaged to every ten nanometers in order to remove some of the noise from the spectrum. Multiplicative Scatter Correction (MSC) was performed on the data in order to compensate for multiplicative scatter effects in the data. Scatter effects are those effects that are caused by physical characteristics, for example surface roughness, as opposed to effects caused by chemical properties. Principle Component Analysis (PCA) was then performed in order to determine any spectral outliers. After all spectral outliers were identified and removed, projection to latent structures (PLS), also known as partial least squares, regression was performed in order to obtain a correlation between the physical properties and the spectra. The regression models were refined by excluding outliers from the data set. The outliers were detected by a warning list from the software and by referencing notes of physical defects that were taken on each sample before they were tested.

Statistical analysis provided correlations of the physical properties on both the whole samples and the ground samples. For each of the three properties, three different data sets were created: raw spectral data, first derivative of the spectral data, and second derivative of the spectral data (Figure 3.1–3.3). All derivation was done by the software. For each of the data sets, six different spectral ranges were considered in order to determine the feasibility of data collection. The six spectral ranges are:

1. 350 – 2500 nm. (Full Range)
2. 1000 – 2400 nm.
3. 650 – 1050 nm.
4. 950 – 1850 nm.
5. 1950 – 2400 nm.
6. Jack-Knifing

Generally, the beginning and end of the spectrum contains random variations that do not contain any information, or what is referred to as noise. The spectral range of 1000 – 2400nm was created in order to analyze the effects of removing the noise. The spectral ranges of 650 – 1050nm, 950 – 1850nm, and 1950 – 2400nm were created to simulate less expensive, lightweight spectrometers. Jack-Knifing is a technique that determines which spectral values are most influential in constructing the regression models. Once the most influential values were determined, a spectral range was created with the Jack-Knifing values plus or minus twenty-five nanometers.

3.2 Modulus of Elasticity

The modulus of elasticity (MOE) ranged in value from a minimum value of 1132 ksi to a maximum value of 3180 ksi. All of the models resulted in good correlations. The

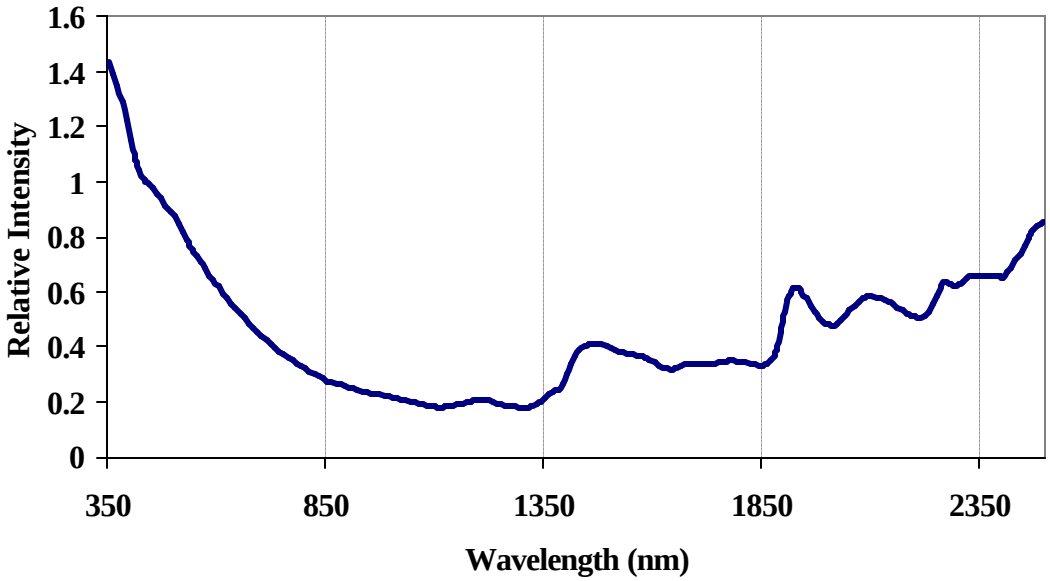

Figure 3.1 – Graphical representation of a typical raw spectral data.

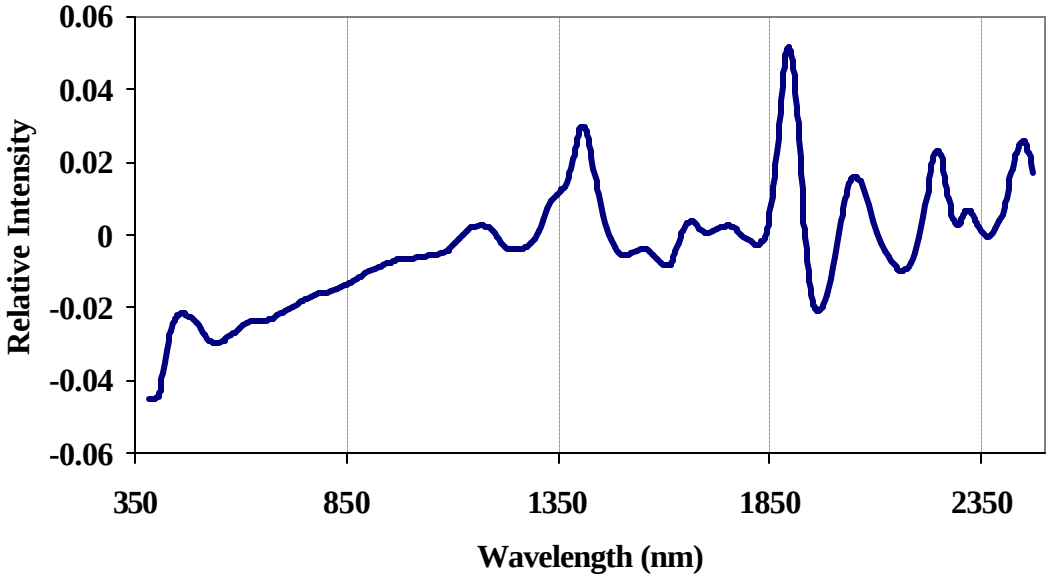

Figure 3.2 – Graphical representation of a typical first derivative spectral data.

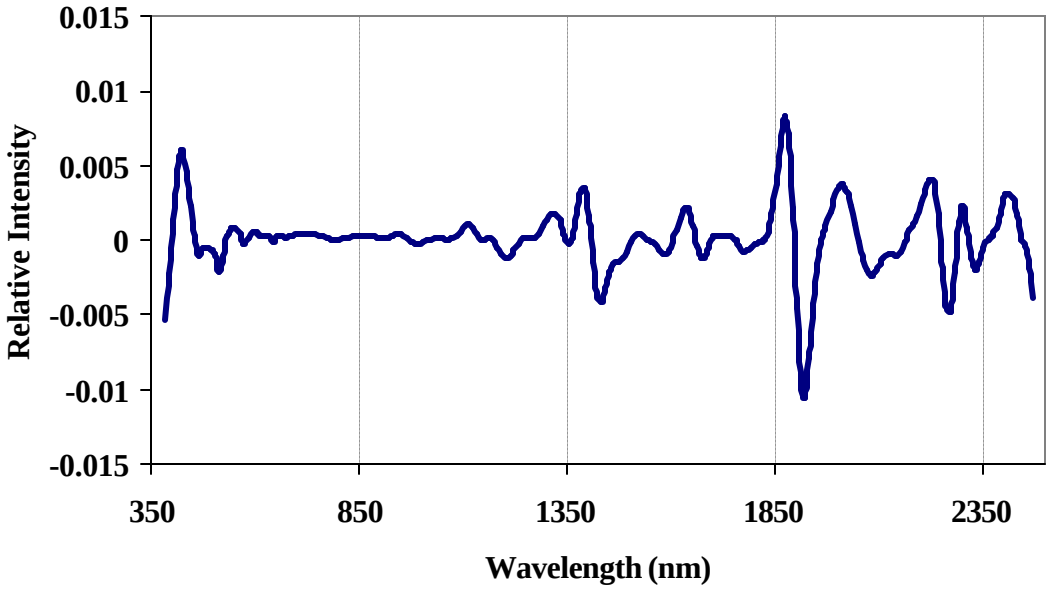

Figure 3.3 – Graphical representation of a typical second derivative spectral data.

correlations of all PLS models are displayed in Table 3.1. The data of the first derivative of the spectra for the whole samples is shown in Figures 3.4 – 3.10. Plots for the raw data and second derivative are similar but the correlations are slightly lower.

The results shown in Figure 3.4 indicate that there was a very good correlation (r = 0.93) between MOE and the first derivative of the full NIR spectra. Figure 3.5 illustrates that removing the initial and final noise from the spectra resulted in a good correlation, but does not improve the results over the full spectra. Figures 3.6, 3.7, 3.8 represent the regression models of the reduced wavelength 650 – 1050nm, 950 – 1850nm, and 1950 – 2400nm, respectively. The 950 – 1850nm reduced wavelength demonstrated the best correlation to the MOE with an r-value of 0.90. The Jack-Knifing technique for the first derivative obtained seven important spectra correlated to predicting MOE. These spectra are 750, 1285, 1475, 1615, 1900, 2085 and 2200 nm (±25nm) as illustrated in Figure 3.9. Figure 3.10 displays there was little reduction in the correlation (r =0.90) as compared to the full spectra. This find proves to be very significant because it opens up these NIR techniques to be able to use very low cost, lightweight spectrometers that read specific spectra.

3.3 Tensile Strength

The tensile strength parallel to the grain ranged in value from a minimum of 7,150 psi to a maximum value of 26,730 psi. The correlations between tensile strength and the NIR spectra were not as good as those for the modulus of elasticity but overall were still significant.

Table 3.1: MOE correlation (r) from all data sets for ground and whole samples.

	Spectral Ranges (nm)					
	Full	**1000 – 2400**	**650 – 1050**	**950 – 1850**	**1950 – 2400**	**Jack-Knife**
MOE - Whole Samples						
Raw Data	0.91	0.91	0.79	0.91	0.83	0.89
1st Derivative	0.93	0.92	0.81	0.90	0.84	0.90
2nd Derivative	0.89	0.91	0.78	0.90	0.83	0.90
MOE - Ground Samples						
Raw Data	0.89	0.88	0.79	0.89	0.87	0.76
1st Derivative	0.91	0.91	0.79	0.88	0.90	0.89
2nd Derivative	0.87	0.89	0.73	0.89	0.89	0.89

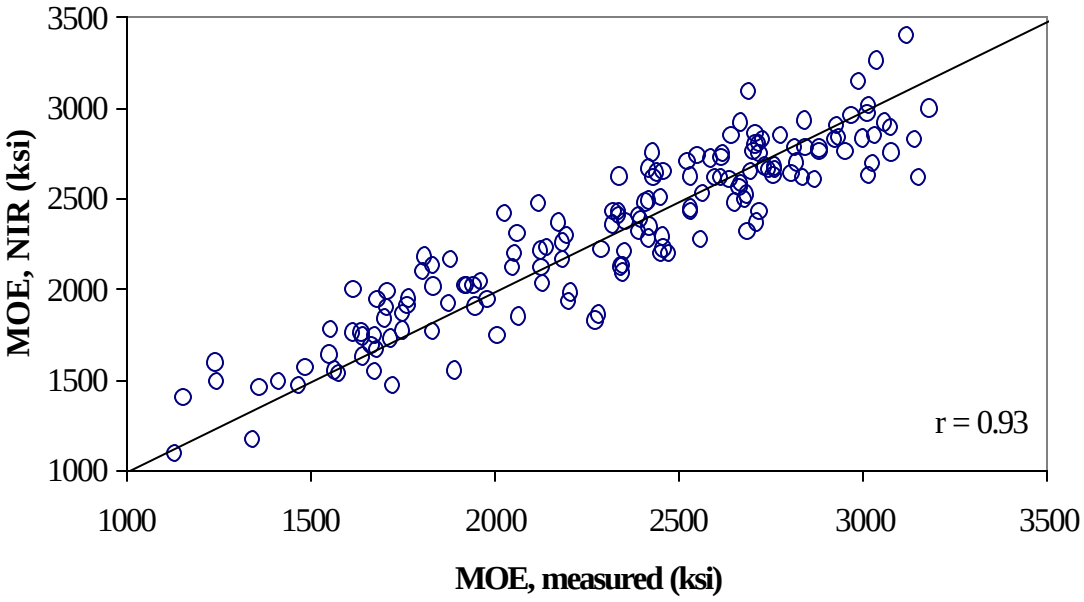

Figure 3.4 – Relationship between first derivative of full spectrum NIR determined MOE and measured MOE.

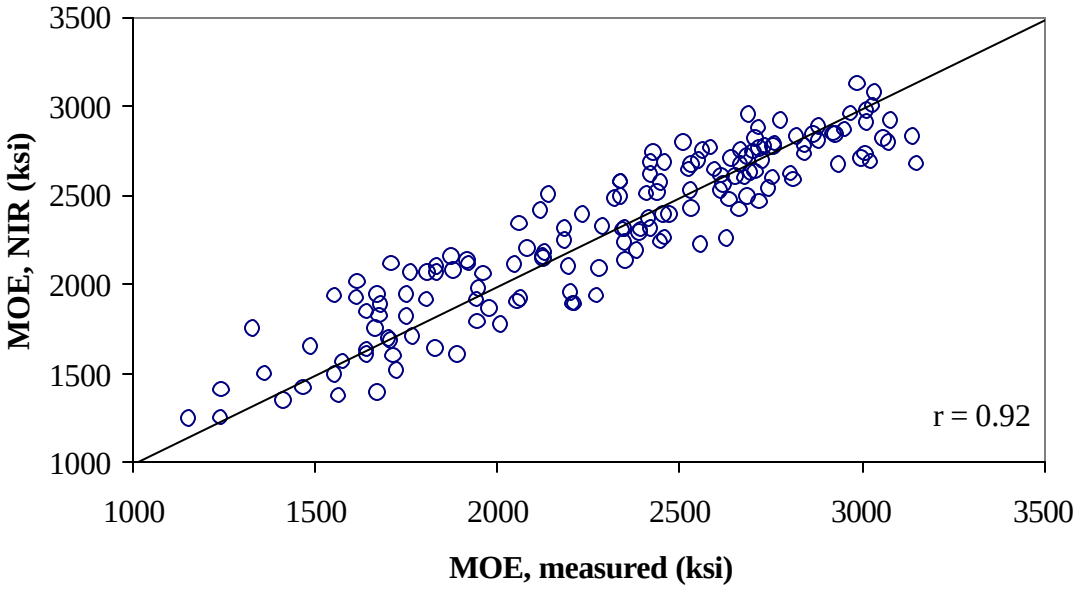

Figure 3.5 – Relationship between first derivative of 1000 – 2400nm NIR determined MOE and measured MOE.

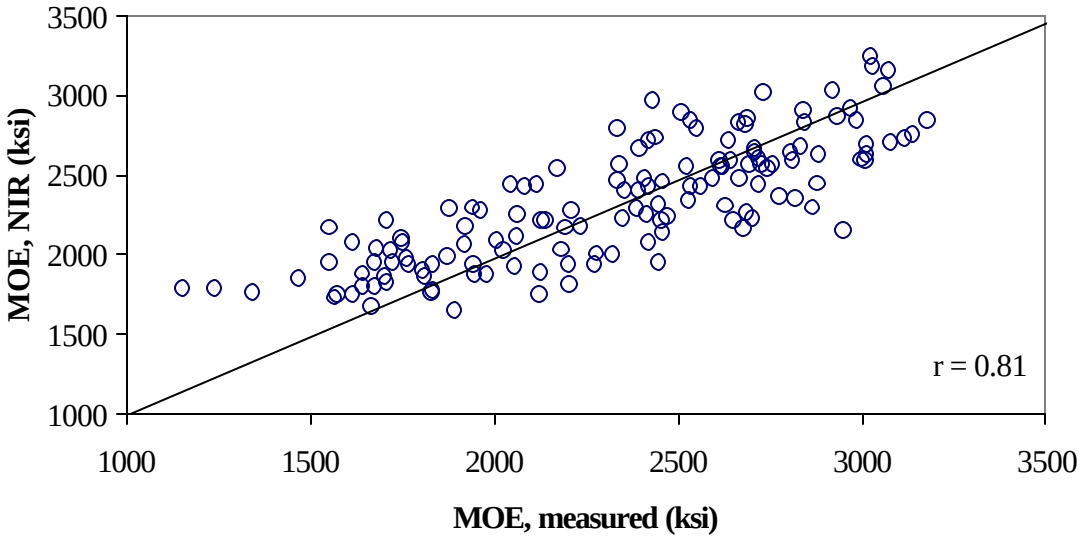

Figure 3.6 – Relationship between first derivative of 650 – 1050nm NIR determined MOE and measured MOE.

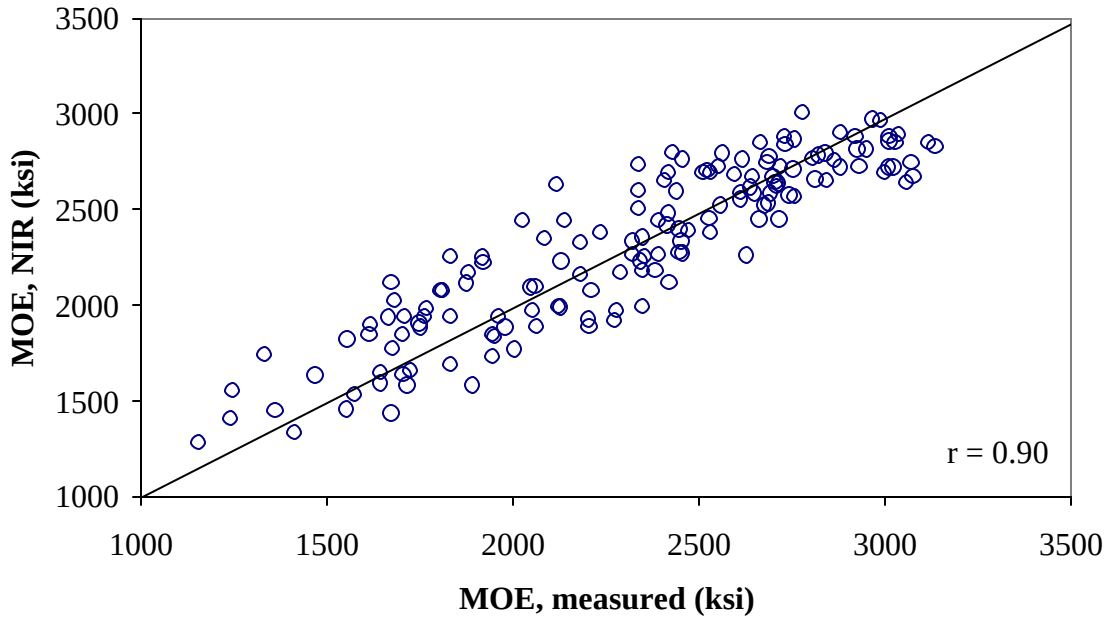

Figure 3.7 – Relationship between first derivative of 950 - 1850nm NIR determined MOE and measured MOE.

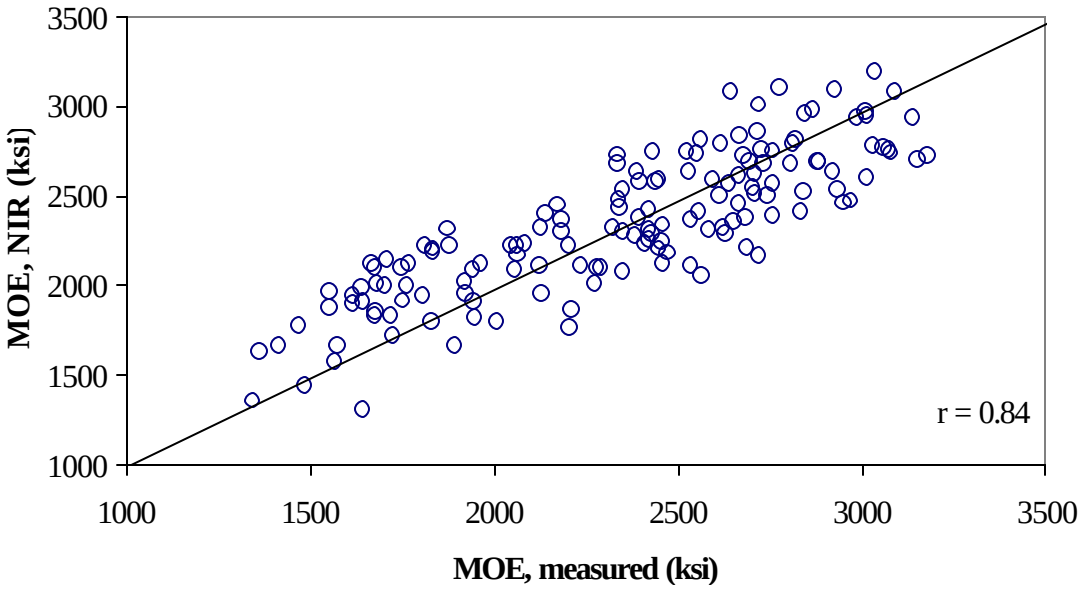

Figure 3.8 – Relationship between first derivative of 1950 - 2400nm NIR determined MOE and measured MOE.

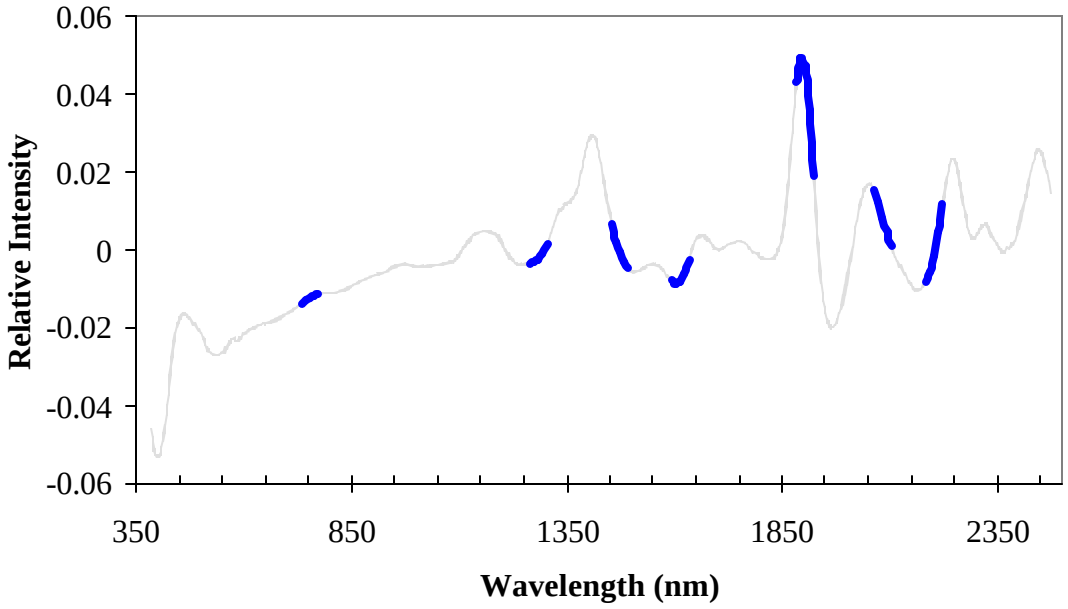

Figure 3.9 – Graphical representation of the first derivative spectral ranges determined from the Jack-Knifing technique.

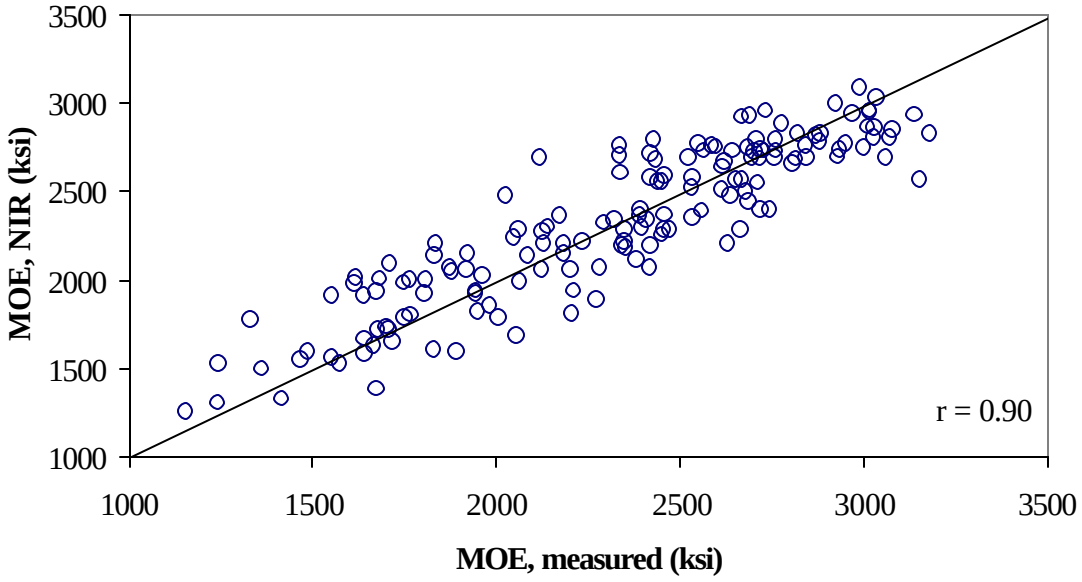

Figure 3.10 – Relationship between first derivative of NIR Jack-Knifing determined MOE and measured MOE.

One reason for the lower tensile correlation is that the stiffness (MOE) of a specimen is not as sensitive to defects such as decay, knots, cross grain and minute checking as is the tensile strength (Wangaard 1950). In addition, tensile failure occurs by a complex combination of two modes, cell-to-cell slippage and cell wall failure. Slippage occurs when two adjacent cells slide past one another, while cell wall failure involves a rupture within the cell wall (Ritter 1990). Thus explaining why the specimens did not break cleanly as was first expected. Figure 3.11 is an example of a typical failed specimen.

The correlations of all PLS models are displayed in Table 3.2. The first derivative of the NIR spectra for the whole samples is shown in Figures 3.12 – 3.18. Plots for the raw data and second derivative are similar but the correlations are lower.

The results shown in Figure 3.12 shows there is significant correlation ($r = 0.78$) between tensile strength and the first derivative of the full NIR spectra. Figure 3.13 illustrates that removing the noise from the spectra does not produce any better correlation ($r = 0.72$) than the full spectra. Figure 3.14, 3.15 and 3.16 represents the regression models of the reduced wavelengths 650 – 1050nm, 950 – 1850nm and 1950 – 2400nm, respectively. The 950 – 1850nm wavelength demonstrated the best correlation of the three; producing the same r-value as the full spectrum, 0.78. The Jack-Knifing technique for the first derivative obtained four important spectra correlated to predicting the tensile strength. These spectra are 400, 1485, 1615 and 1900nm (± 25nm) as illustrated in Figure 3.17. Figure 3.18 demonstrates a very good correlation ($r = 0.76$) compared to the correlation to the full spectra.

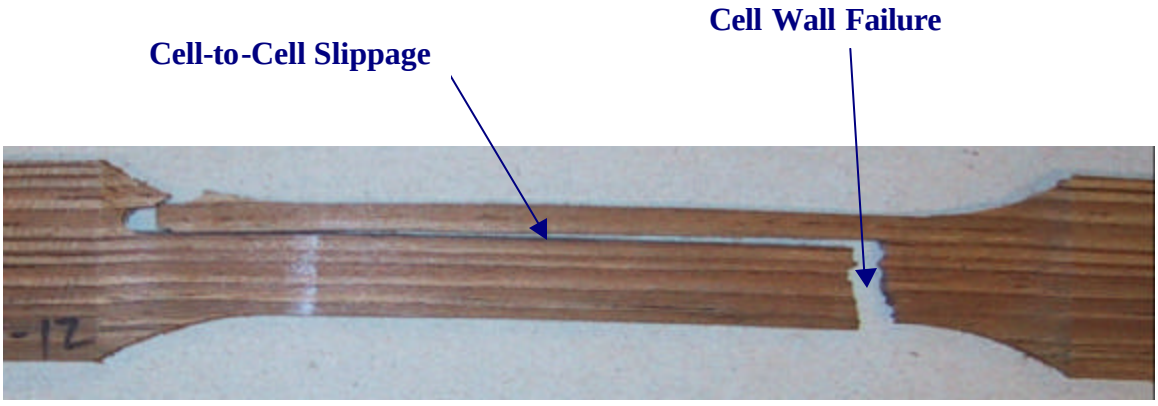

Figure 3 .11 – Typical failure of tensile specimen illustrating cell-to-cell slippage and cell wall failure.

Table 3.2: Tensile strength correlation (r) from all data sets for ground and whole samples.

	Spectral Ranges (nm)					
	Full	**1000 – 2400**	**650 – 1050**	**950 – 1850**	**1950 – 2400**	**Jack-Knife**
Tensile Strength - Whole Samples						
Raw Data	0.79	0.72	0.54	0.73	0.60	0.74
1st Derivative	0.78	0.72	0.49	0.78	0.60	0.75
2nd Derivative	0.76	0.73	0.65	0.72	0.56	0.73
Tensile Strength - Ground Samples						
Raw Data	0.73	0.69	0.63	0.69	0.68	0.71
1st Derivative	0.75	0.66	0.64	0.70	0.63	0.74
2nd Derivative	0.68	0.66	0.56	0.69	0.57	0.69

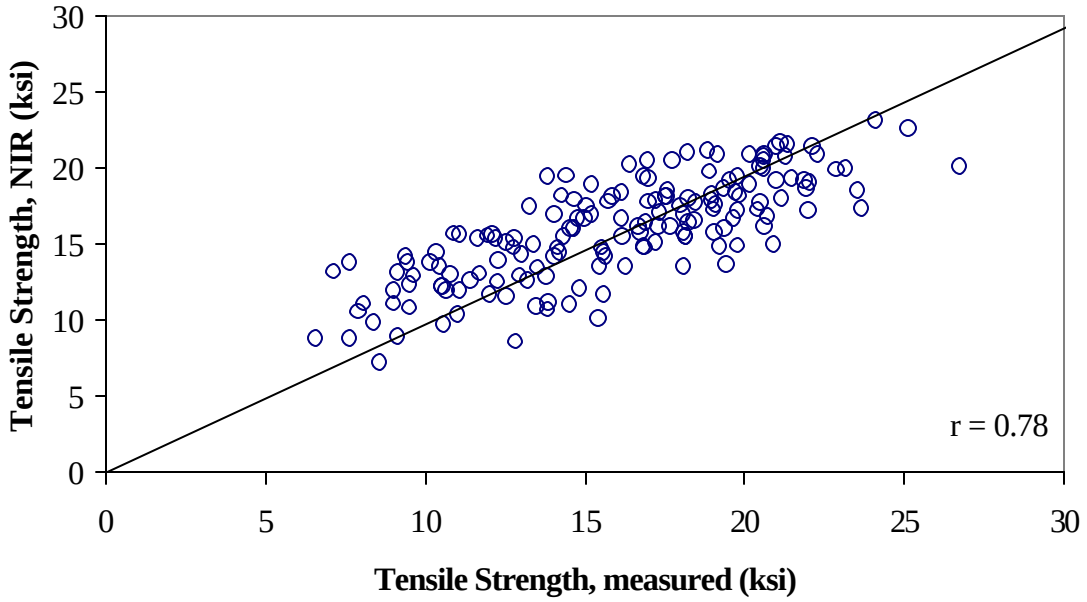

Figure 3.12 – Relationship between first derivative full spectra NIR determined Tensile Strength and measured Tensile Strength.

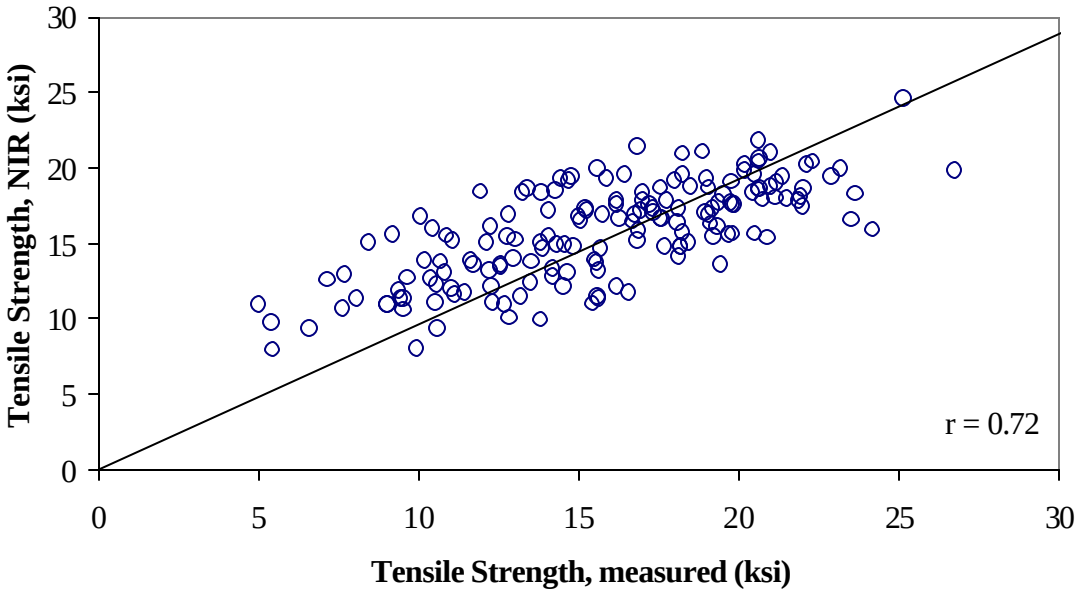

Figure 3.13 – Relationship between first derivative 1000 – 2400nm NIR determined Tensile Strength and measured Tensile Strength.

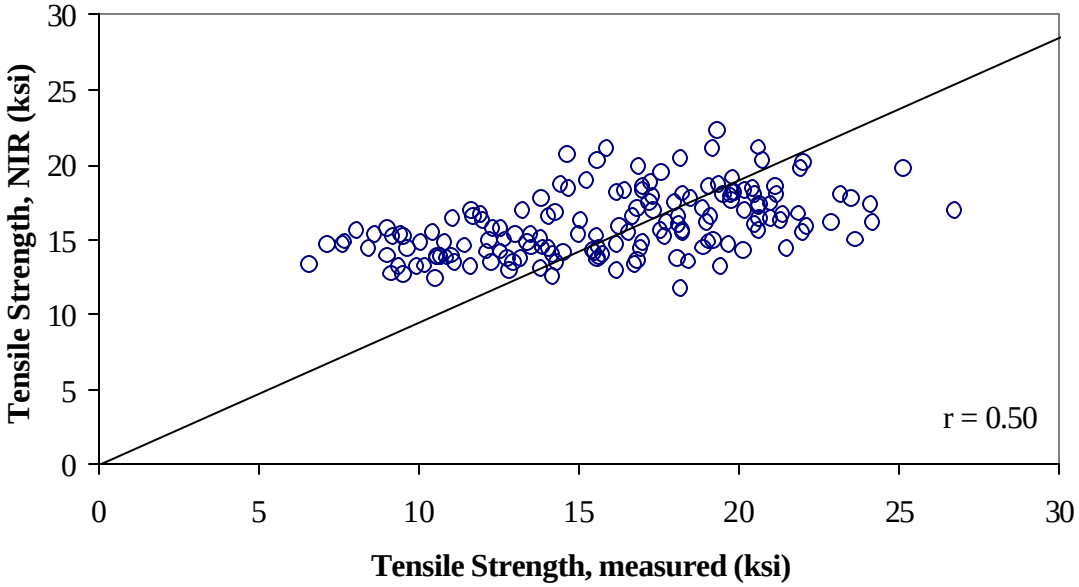

Figure 3.14 – Relationship between first derivative 650 – 1050nm NIR determined Tensile Strength and measured Tensile Strength.

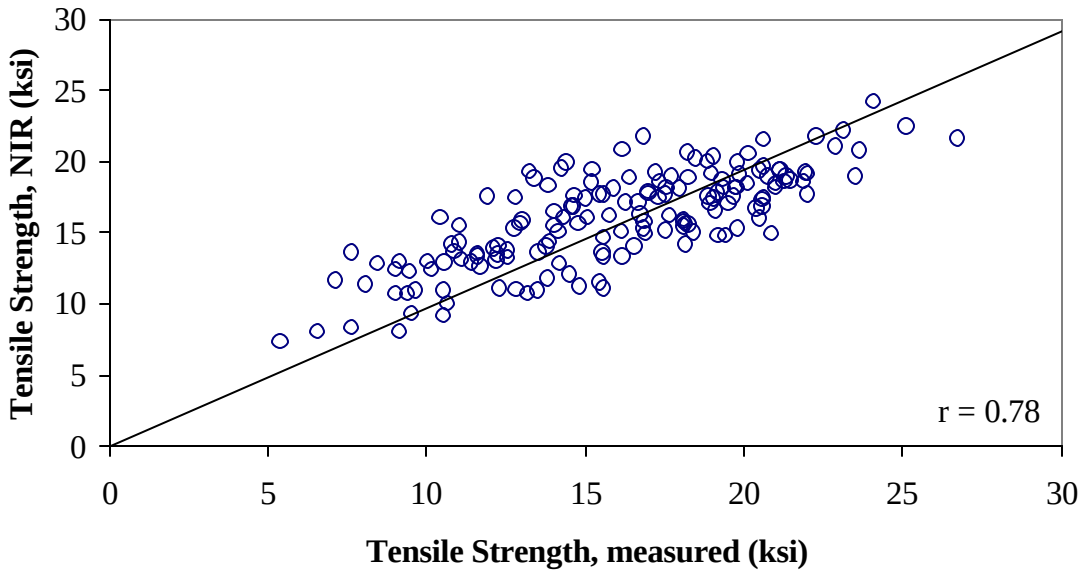

Figure 3.15 – Relationship between first derivative 950 – 1850nm NIR determined Tensile Strength and measured Tensile Strength.

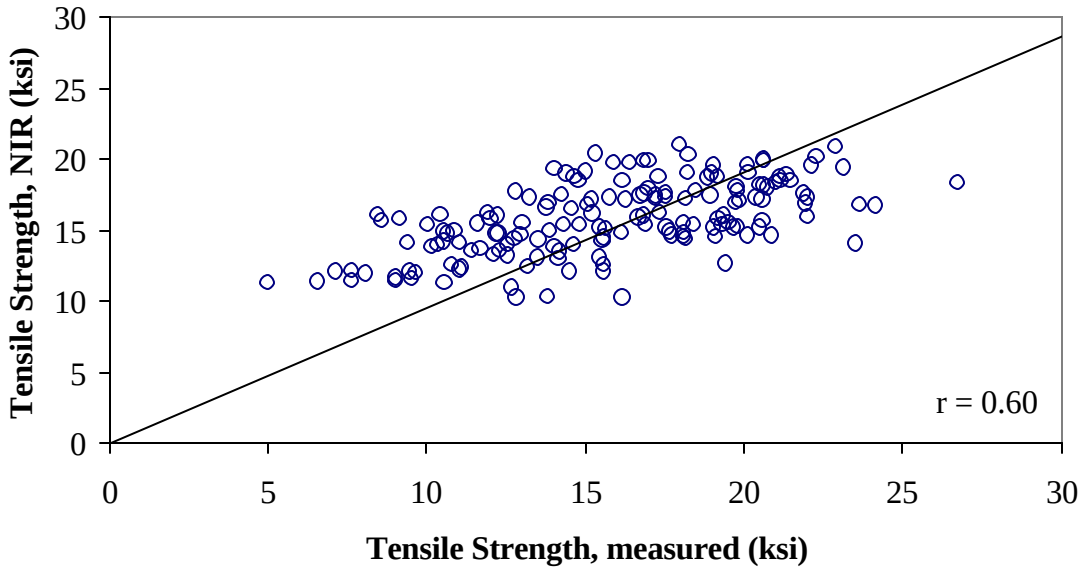

Figure 3.16 – Relationship between first derivative 1950 – 2400nm NIR determined Tensile Strength and measured Tensile Strength.

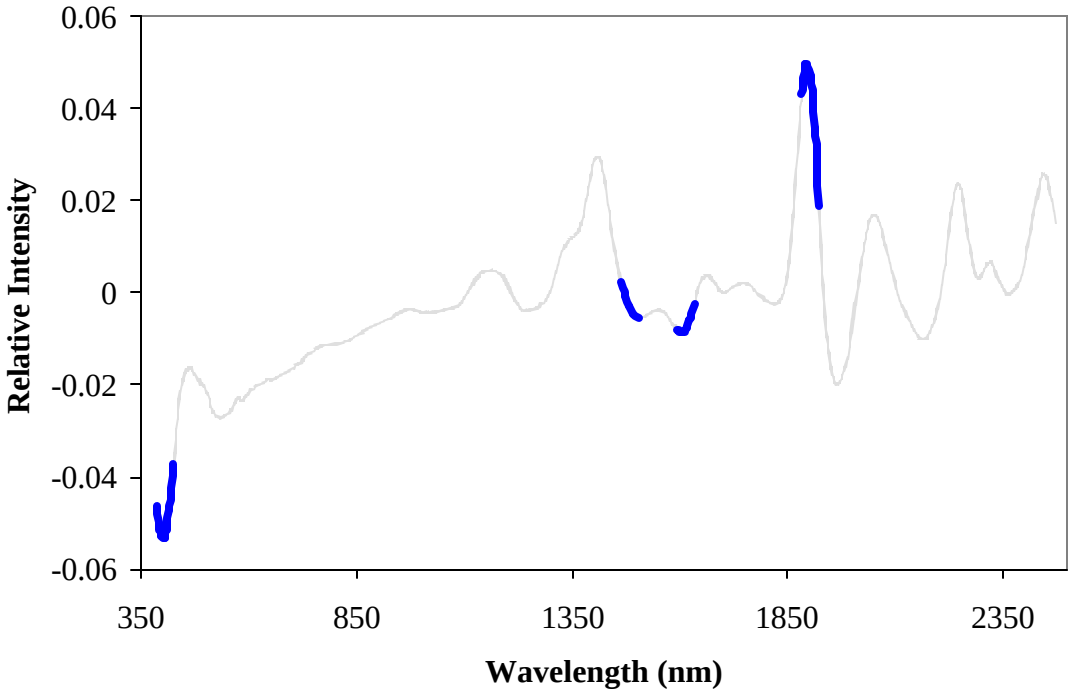

Figure 3.17 – Graphical representation of the first derivative spectral ranges determined from the Jack-Knifing technique.

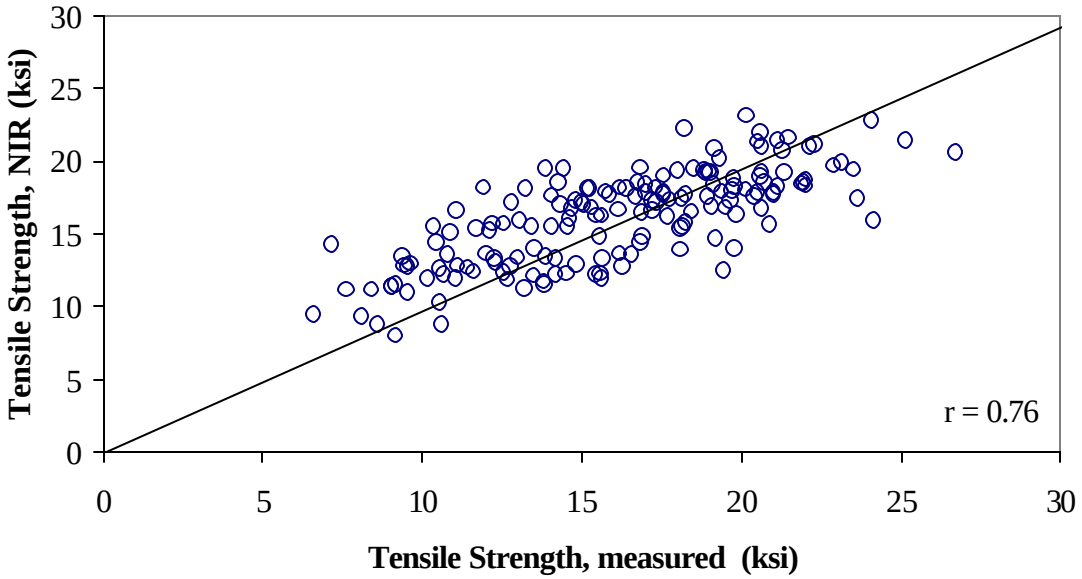

Figure 3.18 – Relationship between first derivative Jack-Knifing NIR determined Tensile Strength and measured Tensile Strength.

3.4 Creosote Content

The creosote content ranged in value from a minimum value of 1.70 percent to a maximum value of 6.23 percent. The models for the ground samples resulted in excellent correlations, while the models for the whole samples were quite poor. One explanation for this is the creosote content was extracted from the ground samples, which behave more as a homogeneous material, whereas the wholes samples could contain patches of high and low creosote content. The correlations of all PLS models are displayed in Table 3.3. The data of the first derivative of the spectra for the ground samples is shown in Figures 3.19 – 3.25. Plots for the raw data and second derivative are similar but the correlations are lower.

The results shown in Figure 3.19 indicate that there is excellent correlation (r = 0.96) between creosote content and the first derivative of the full NIR spectra of the ground samples. Figure 3.20 illustrates that removing the initial and final noise from the spectra results in a poorer correlation (r = 0.76) compared to the full spectra. Figures 3.21, 3.22, 3.23 represent the regression models of the reduced wavelength 650 – 1050nm, 950 – 1850nm, and 1950 – 2400nm, respectively. The 950 – 1850nm reduced wavelength demonstrated the best correlation to the MOE with an r-value of 0.87. The Jack-Knifing technique for the first derivative obtained four important spectra correlated to predicting MOE. These spectra are 665, 1215, 1735 and 2435nm (±25nm) as illustrated in Figure 3.24. Figure 3.25 show that the Jack-Knifing techniques did not produce a very good correlation (r =0.52).

Table 3.3: Creosote correlation (r) from all data sets for ground and whole samples.

	Spectral Ranges (nm)					
	Full	**1000 – 2400**	**650 – 1050**	**950 – 1850**	**1950 – 2400**	**Jack-Knife**
Creosote Whole Samples						
Raw Data	0.21	0.24	0.21	0.24	0.28	0.00
1st Derivative	0.30	0.48	0.25	0.33	0.53	0.64
2nd Derivative	0.28	0.53	0.40	0.52	0.51	0.56
Creosote Ground Samples						
Raw Data	0.95	0.85	0.36	0.85	0.37	0.37
1st Derivative	0.96	0.76	0.44	0.87	0.36	0.52
2nd Derivative	0.87	0.36	0.49	0.89	0.37	0.41

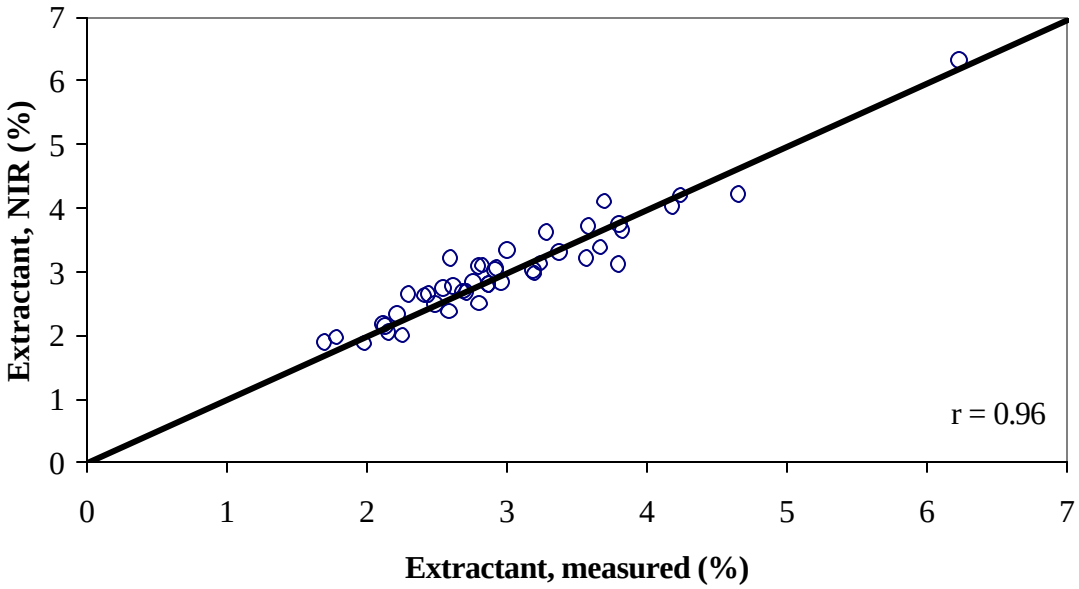

Figure 3.19 – Relationship between first derivative full spectra NIR determined Extractant percentage and measured Extractant percentage.

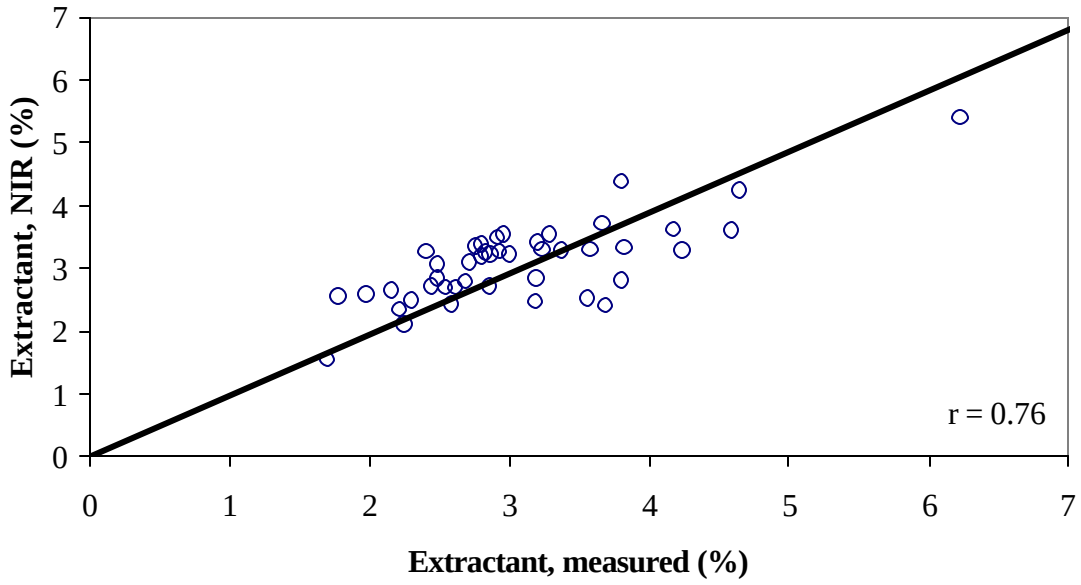

Figure 3.20 – Relationship between first derivative 1000 – 2400nm NIR determined Extractant percentage and measured Extractant percentage.

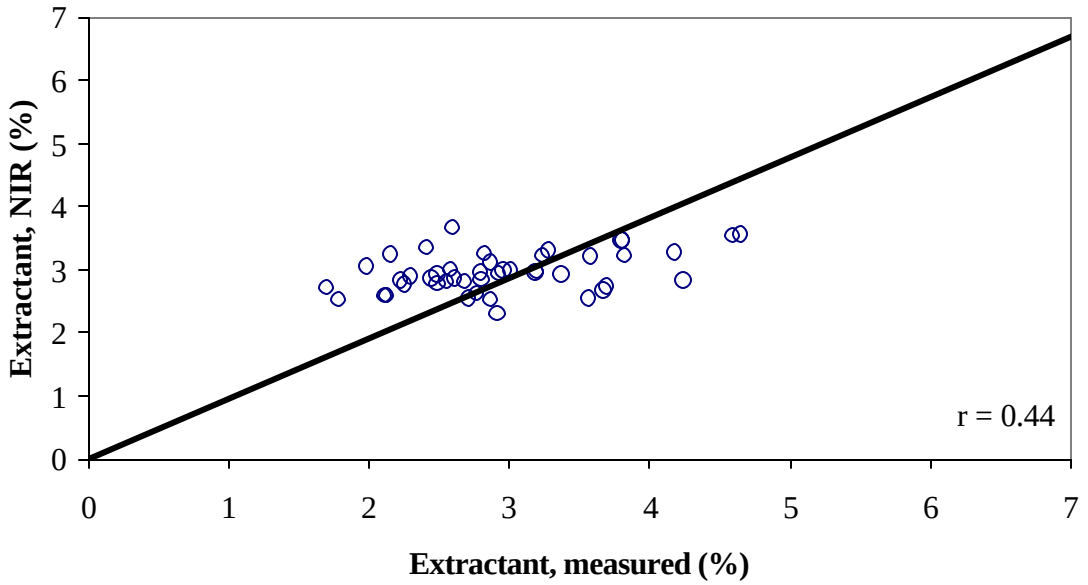

Figure 3.21 – Relationship between first derivative 650 – 1050nm NIR determined Extractant percentage and measured Extractant percentage.

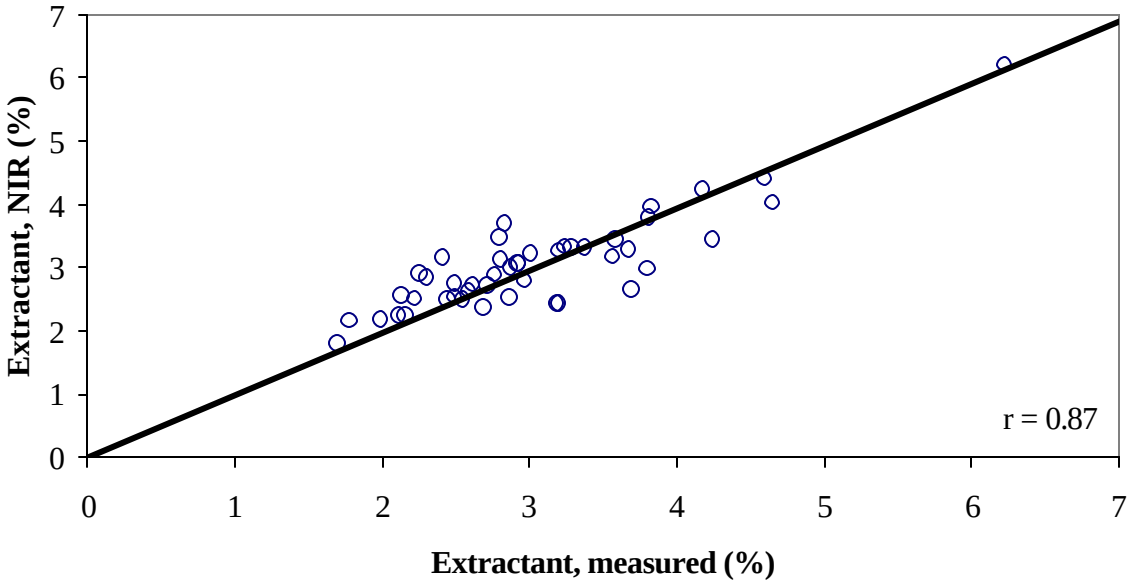

Figure 3.22 – Relationship between first derivative 950 – 1850nm NIR determined Extractant percentage and measured Extractant percentage.

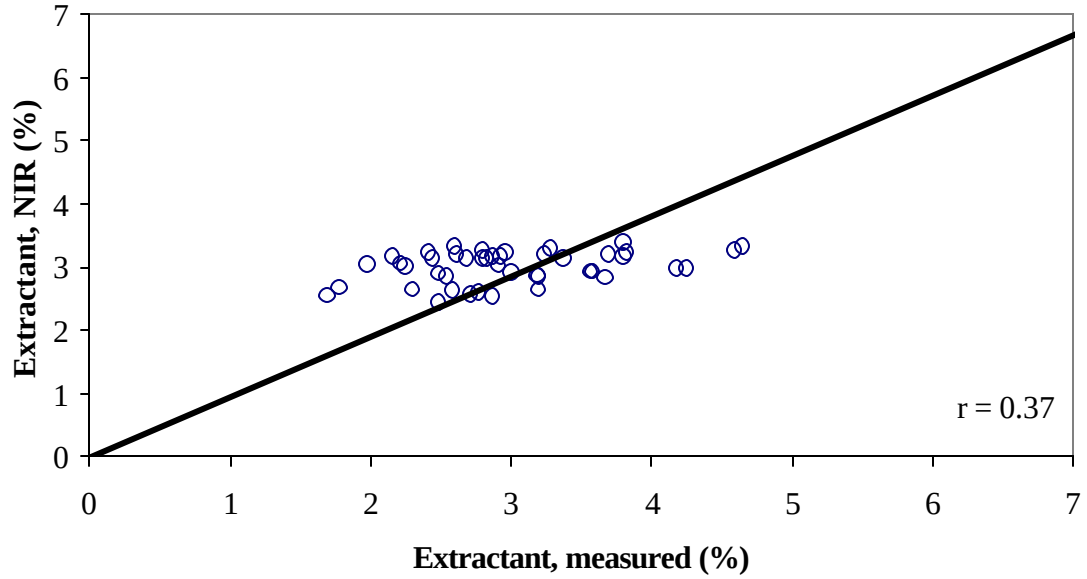

Figure 3.23 – Relationship between first derivative 1950 – 2400nm NIR determined Extractant percentage and measured Extractant percentage.

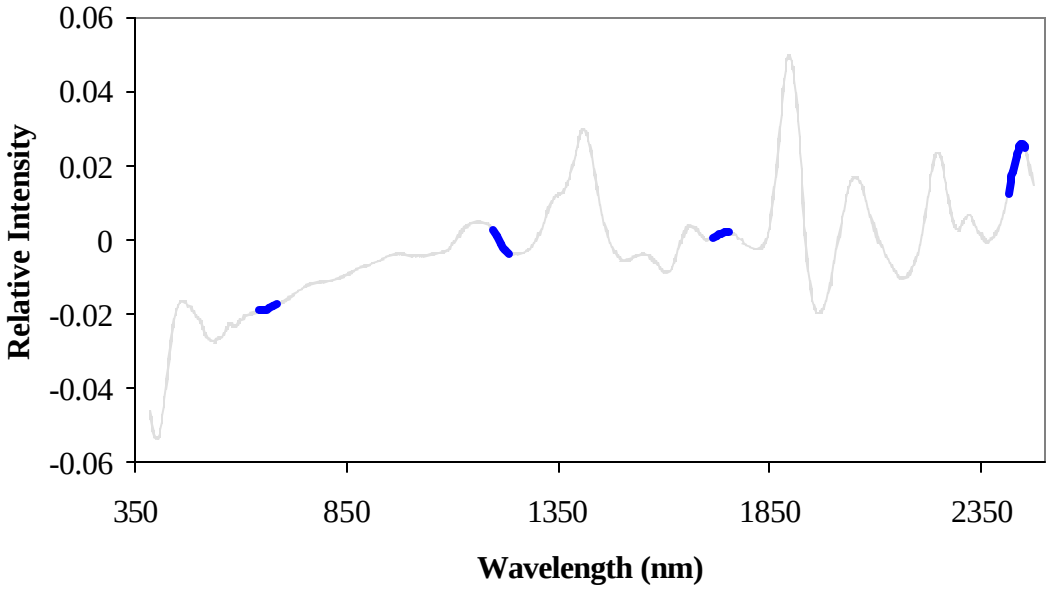

Figure 3.24 – Graphical representation of the first derivative spectral ranges determined from the Jack-Knifing technique.

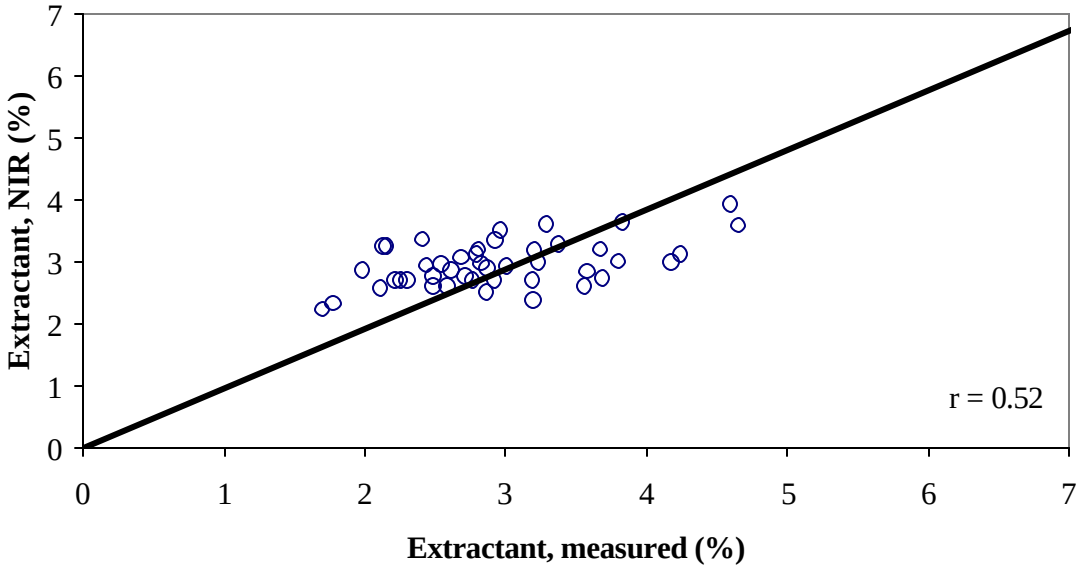

Figure 3.25 – Relationship between first derivative Jack-Knifing NIR determined Extractant percentage and measured Extractant percentage.

3.5 Other Comparisons

General comparisons between tensile strength, modulus of elasticity and creosote content were also considered. Figure 3.26 shows a significant correlation ($r = 0.75$) between tensile strength and modulus of elasticity. All 185 samples except for those removed as outlier were considered. Figure 3.27 and Figure 3.28 display relationships between modulus of elasticity and tensile strength versus predicted creosote content, respectively. Both graphs illustrate that as the creosote content increases the modulus of elasticity and tensile strength decrease.

Comparisons of tensile strength, modulus of elasticity and creosote content of the samples versus the samples' location on the cross section and location on the pole were also consider. Figure 3.29 and Figure 3.30 display relationships between the modulus of elasticity of the inner and outer samples versus the cross sectional location, respectively. Figure 3.31 and Figure 3.32 display relationships between the tensile strength of the inner and outer samples versus the cross sectional location, respectively. Figure 3.33 and Figure 3.34 display relationships between creosote content of the inner and outer samples determined from NIR models versus the cross sectional location, respectively. Figure 3.35 displays the relationship between the average modulus of elasticity of the inner and outer samples of each section versus the location on the pole. Figure 3.36 displays the relationship between the average tensile strength of the inner and outer samples of each section versus the location on the pole. Figure 3.37 displays the relationship between the average creosote content of the inner and outer samples of each section versus the location on the pole.

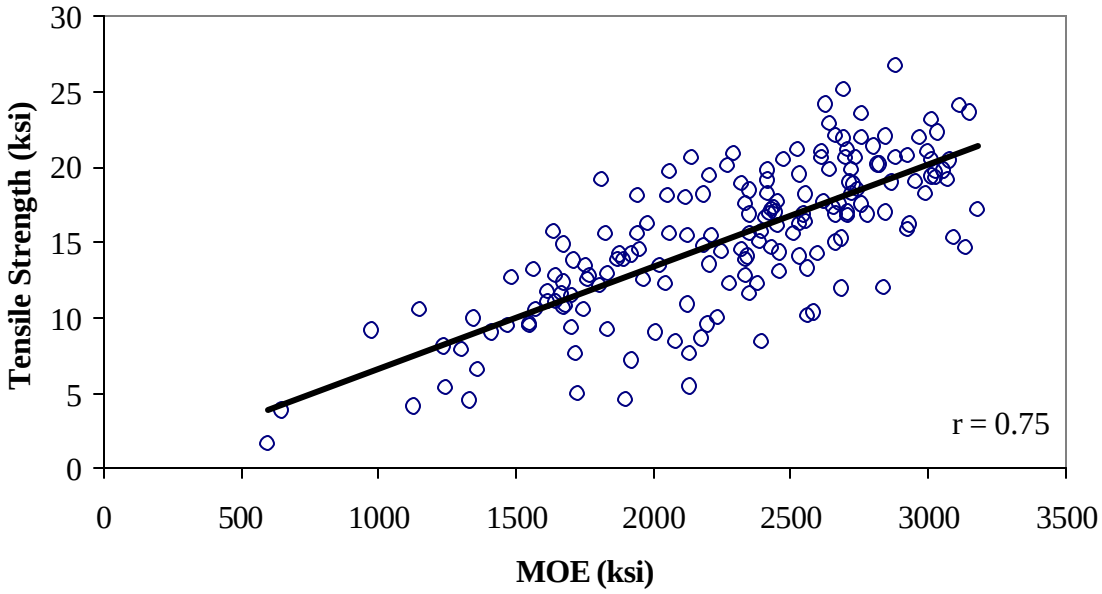

Figure 3.26 – Relationship between measured Tensile Strength versus measured Modulus of Elasticity with outliers removed.

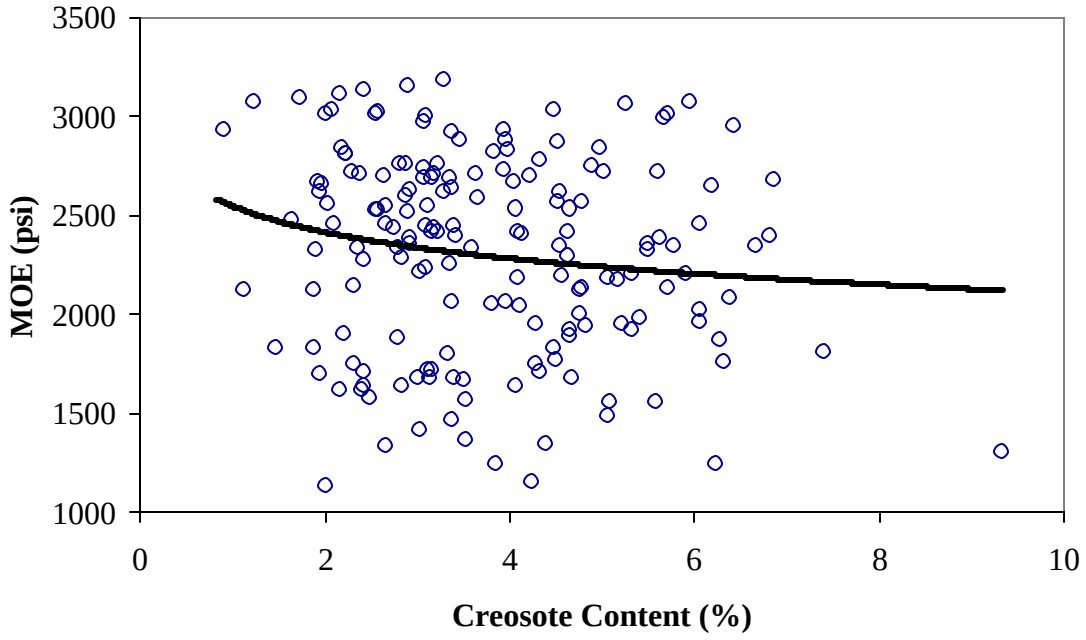

Figure 3.27 – Relationship between NIR predicted creosote content versus measured Modulus of Elasticity.

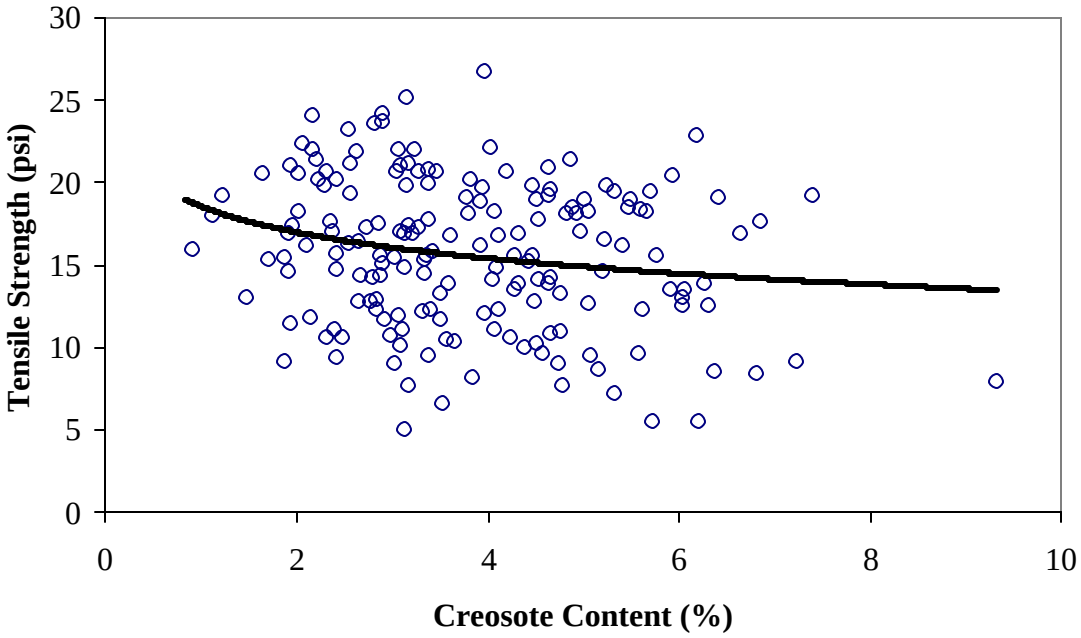

Figure 3.28 – Relationship between NIR predicted creosote content versus measured Tensile Strength.

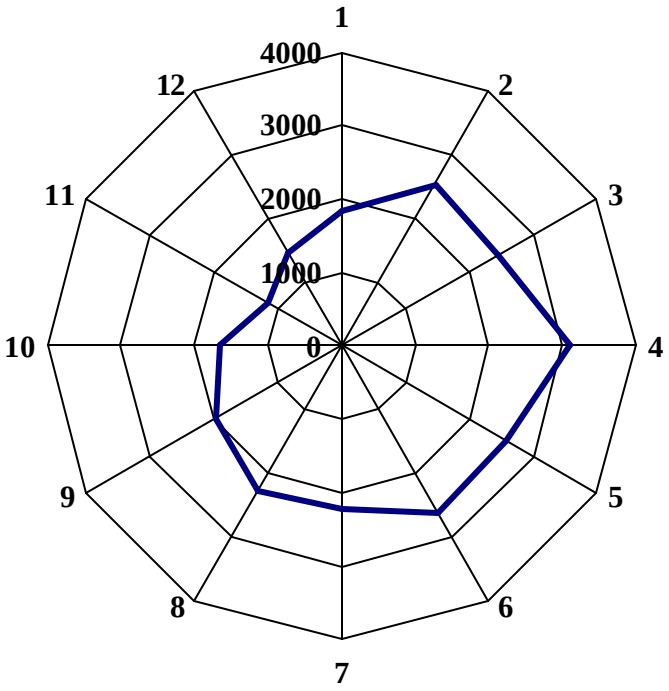

Figure 3.29 – Illustration of average Modulus of Elasticity (ksi) of inner samples versus inner cross sectional location.

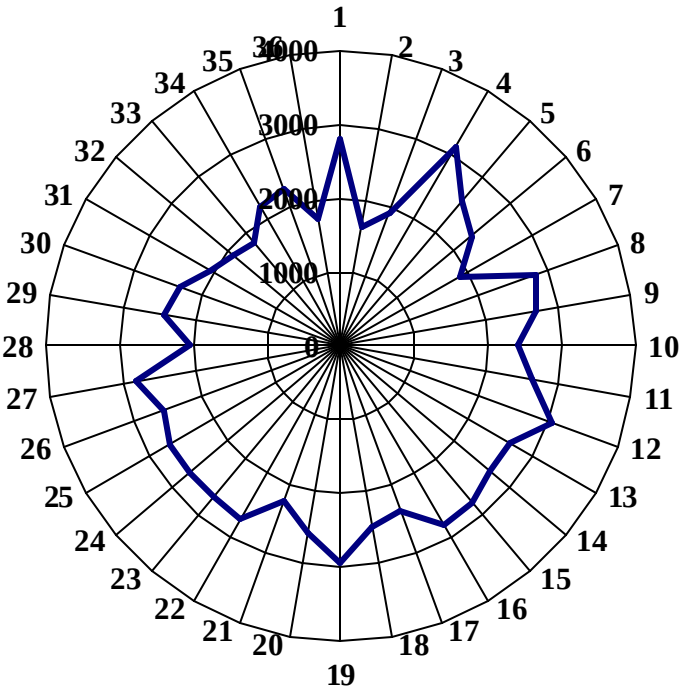

Figure 3.30 – Illustration of average Modulus of Elasticity (ksi) of outer samples versus outer cross sectional location.

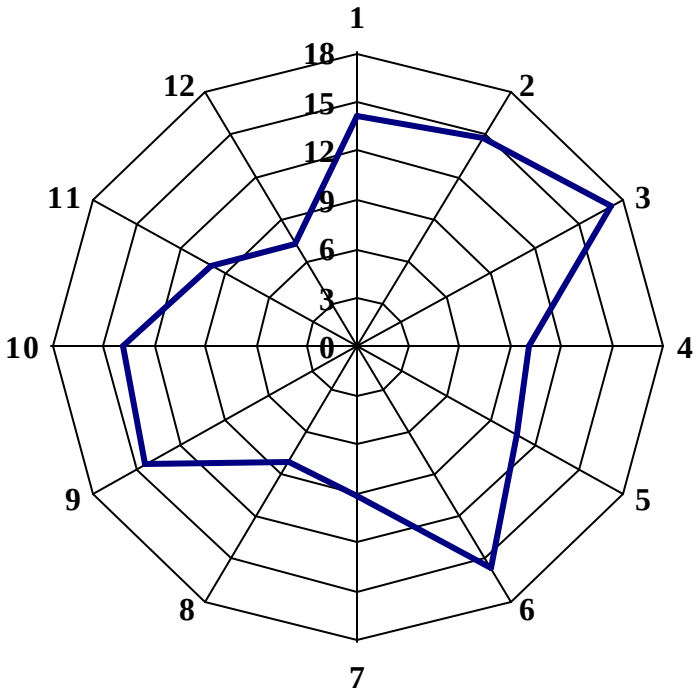

Figure 3.31 – Illustration of average tensile strength (ksi) of inner samples versus inner cross sectional location.

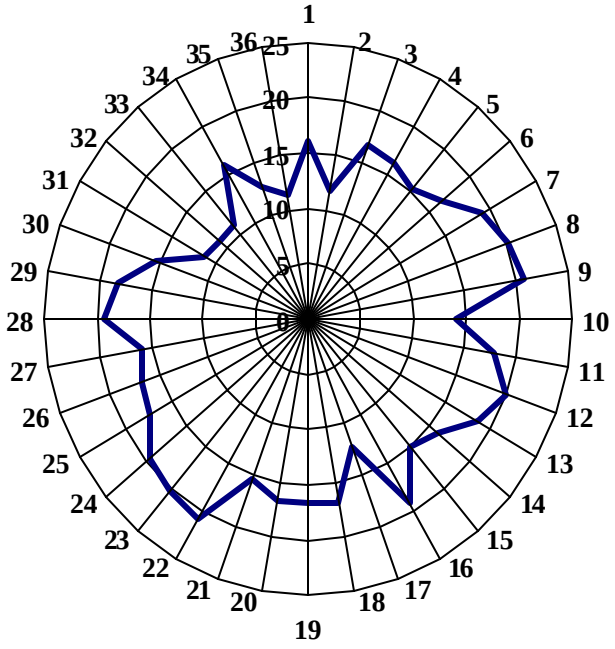

Figure 3.32 – Illustration of average tensile strength (ksi) of outer samples versus inner cross sectional location.

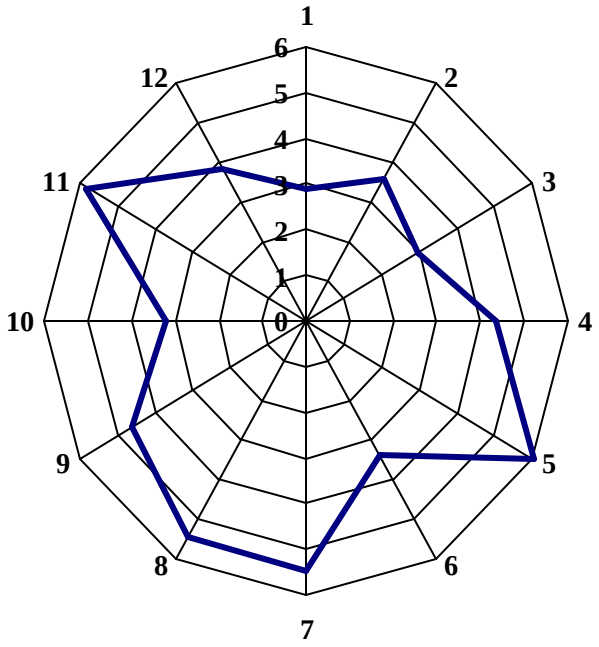

Figure 3.33 – Illustration of creosote content (%) of inner samples versus inner sample location.

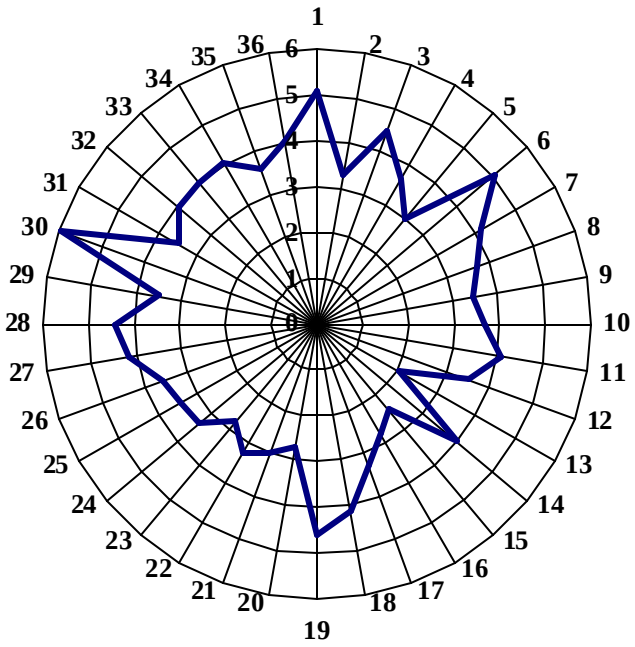

Figure 3.34 – Illustration of creosote content (%) of outer samples versus outer sample location.

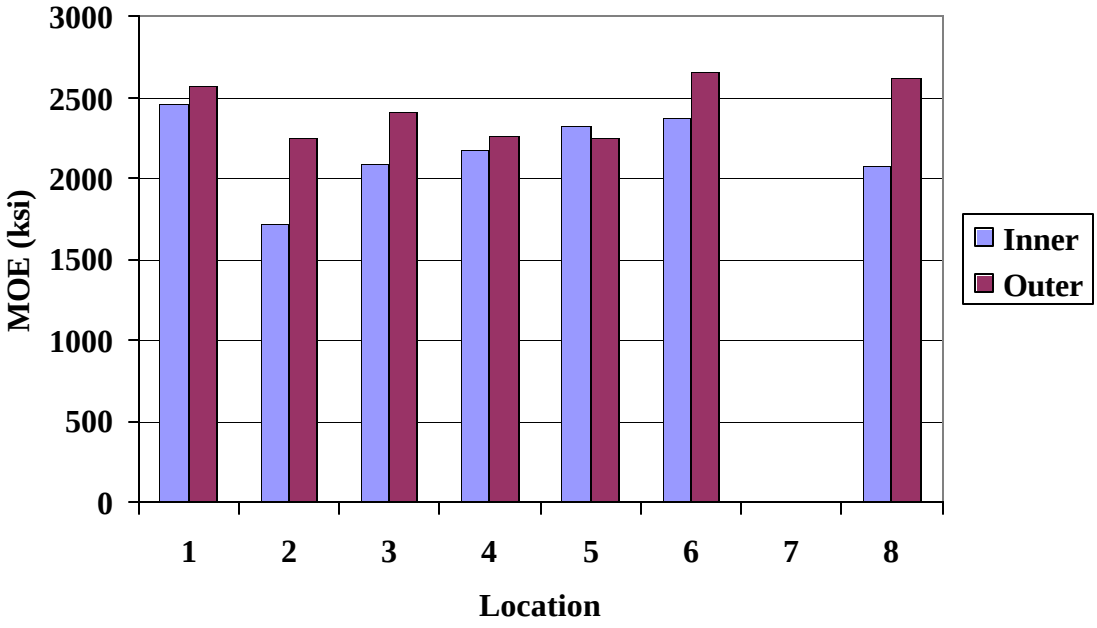

Figure 3.35 – Illustration of average Modulus of Elasticity of each section versus location on the pole.

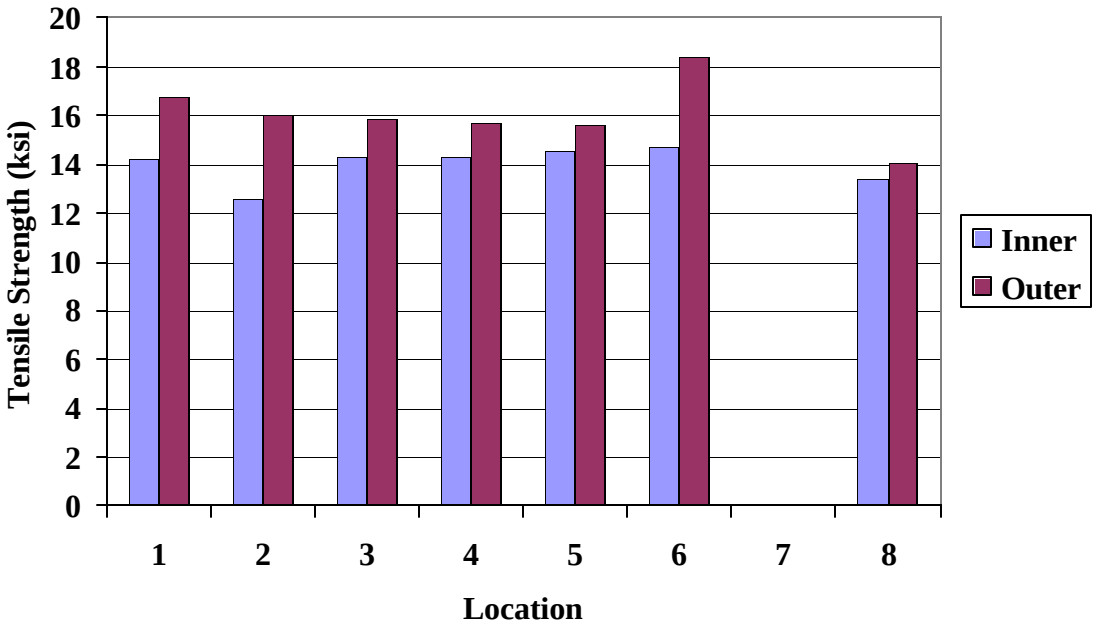

Figure 3.36 – Illustration of Tensile Strength of each section versus location on the pole.

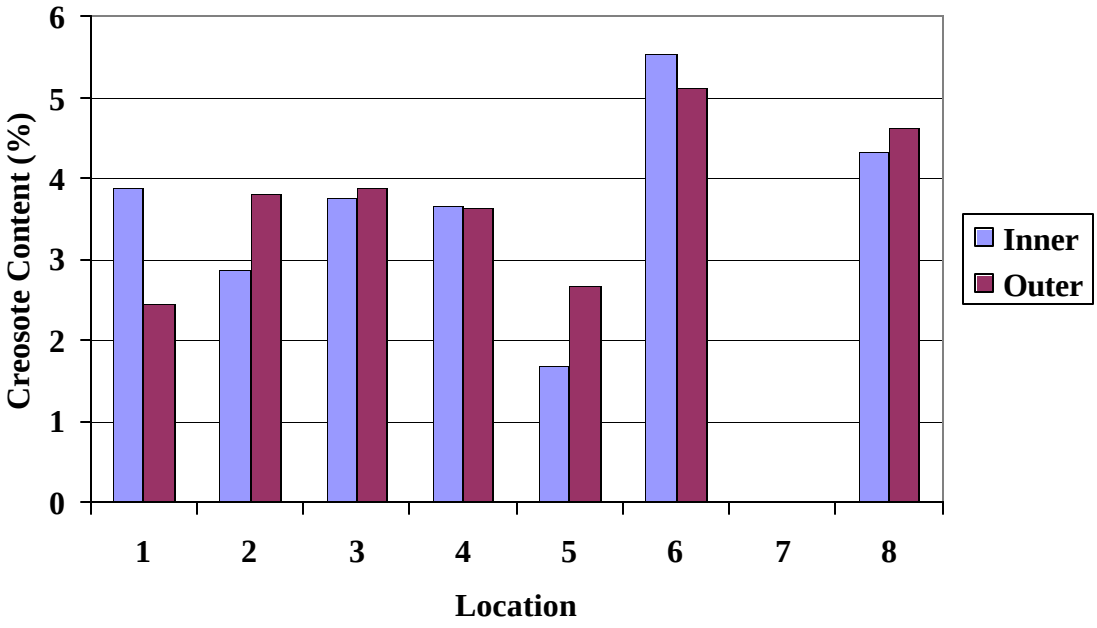

Figure 3.37 – Illustration of predicted Creosote Content of each section versus location on the pole.

3.6 Structural Analysis

The bending strength of a section of the pole can be determined from knowing the tensile strength and modulus of elasticity of the individual specimens. This will demonstrate by obtaining several NIR scans around the pole the flexural strength could be predicted for that section.

Bending results in both tensile and compressive stresses. Therefore, given a design load, P, the allowable tensile stress used in design can be determined based upon the stress distribution on the cross section (Figure 3.38). The maximum bending moments occurs at the base of the pole and can be calculated by the following (Figure 3.39):

$$M_{\max} = P \times L$$

where,

M_{max} = Maximum bending moment produced by load P (in-lb),

P = Design load applied to the pole (lbs),

L = Length from the ground to the location of the load (in.).

The tensile stress occurs on the side of the pole opposite the load. Thus, tensile stress occurring at any location is:

$$q_t = \frac{M_{\max} C_t}{I}$$

where,

Q_t = Maximum tensile stress (psi),

M = Maximum bending moment (in-lb),

Ct = Distance from the neutral axis (NA) to the desired location in tension.

I = Moment of Inertia of the cross section (in^4).

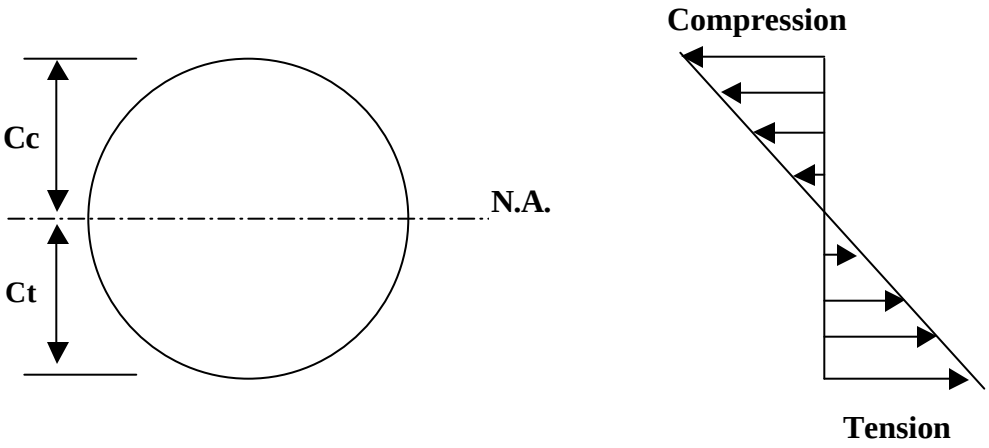

Figure 3.38 – Illustration of the stress distribution due to flexural bending.

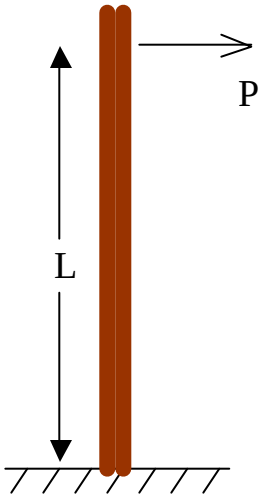

Figure 3.39 – Illustration of the design load acting on the pole causing a maximum bending moment at the base of the pole.

The equations used to calculate the tensile stress are applicable for a member composed of a homogeneous material. Since the modulus of elasticity is not uniform throughout the section, the transformed-section method can be used to predict the bending stresses of the entire pole. This method consists of transforming the cross section of the pole into an equivalent cross section of an imaginary pole composed of a uniform material. This is accomplished by multiplying the width (dimension parallel to the neutral axis) by the modular ratio. The modular ratio is defined by:

$$n = \frac{E_2}{E_1}$$

where,

n = modular ratio,
E_1 = MOE to which the section is transformed,
E_2 = MOE of the specimen being transformed.

This procedure is very complex to solve by hand for a circular cross section. Thus, a computer program would be useful to solve for the transformed cross section. Once this is completed, the transformed section is analyzed in the customary manner for a beam of one material. As a final step, the stresses in the transformed beam are converted to those in the original beam.

Once the allowable tensile stress for a given location is obtain from the design load, the values can then be compared to those obtain from the NIR spectra in order to see if the pole has efficient strength.

3.7 Conclusion

In order to eliminate variables of unknown, future studies need to be done on controlled samples. Regulating the moisture content, creosote content and the amount of time the sample is exposed to fungi could accomplish controlling the samples. Doing so will provide more accurate calibration models and the possibility of determining which chemical properties are driving the mechanical properties.

The mode of failure should also be investigated. For telephone poles and some components of timber bridges such as stringers, bending will be the primary mode of failure. A common failure sequence for wood in simple bending is the formation of minute compression failures followed by the development of macroscopic wrinkles. This effectively results in a sectional increase in the compression zone and a sectional decrease in the tension zone, which is eventually followed by tensile failure (Ritter 1990). Since this occurs it would be advantageous to consider samples in compression parallel to the grain. This would allow for analysis of a pure stress state in order to see if NIR spectra can predict the initial stage of bending failure.

The results of this study indicate that Near Infrared spectroscopy has the potential to predict the mechanical and physical properties of creosote treated timber by means of nondestructive techniques. Models created with the reduced wavelength 950-1850nm and the 50 nm intervals determined by Jack-Knifing show very little loss in prediction capabilities compared to the full spectral range. These findings prove the feasibility of using lightweight, inexpensive instruments to predict the mechanical properties of creosote treated timber.

LIST OF REFERENCES

LIST OF REFERENCES

American Society for Testing Materials. (1999). "Standard Test Methods for Small Clear Specimens of Timber." D 1037–99, West Conshohocken, PA.

American Society for Testing Materials. (2000). "Standard Test Methods for Small Clear Specimens of Timber." D 143–94, West Conshohocken, PA.

AWPI. (1994). The 1994 wood preserving industry production statistical report. American Wood Preservers' Institute. Fairfax, VA.

Micklewright, J.T. (1989). "Wood preservation statistics, 1987." American Wood Preservers' Association Annual Report. AWPA, Granbury, Texas.

Ritter, Micheal A. (1990). *Timber Bridges – Design , Construction, Inspection, and Maintenance*. Forest Service, U.S. Department of Agriculture. Washington, D.C.

Roliadi, H., Hse, C.Y., Choong, E.T., and Shupe, T.F. (2000). "Decay Resistance of Out-of-Service Utility Poles as Related to the Distribution of Residual Creosote Content." 50 (11/12). Forest Product Journal. 64-68.

Ross, R. J., Pellerin, R.F., Volny, N., Salsig, W.W. and Falk, R.H. (1999). *Inspection of Timber Bridges Using Stress Wave Timing Nondestructive Evaluation Tools – A Guide for Use and Interpretation.* Gen. Tech. Rep. FPL-GTR-114. Forest Service, U.S. Department of Agriculture. Forest Products Laboratory. Madison, WI.

Wangaard, F. F. (1950). *The Mechanical Properties of Woods.* John Wiley & Son, Inc. New York, New York.

VITA

Stephen Edward Hedrick II was born in Anchorage, Alaska on July 11, 1978. He attended the local school system in South Point, Ohio, where he graduated from South Point High School in May 1996. He attended West Virginia Institute of Technology, in Montgomery, West Virginia, were he graduated with a Bachelor of Science in Civil Engineering in May 2001. He entered the graduate program in Civil Engineering at the University of Tennessee, in Knoxville, Tennessee, were he graduated with a Master of Science Degree in the August 2003.